

ChemComm

Accepted Manuscript



This is an *Accepted Manuscript*, which has been through the Royal Society of Chemistry peer review process and has been accepted for publication.

Accepted Manuscripts are published online shortly after acceptance, before technical editing, formatting and proof reading. Using this free service, authors can make their results available to the community, in citable form, before we publish the edited article. We will replace this *Accepted Manuscript* with the edited and formatted *Advance Article* as soon as it is available.

You can find more information about *Accepted Manuscripts* in the [Information for Authors](#).

Please note that technical editing may introduce minor changes to the text and/or graphics, which may alter content. The journal's standard [Terms & Conditions](#) and the [Ethical guidelines](#) still apply. In no event shall the Royal Society of Chemistry be held responsible for any errors or omissions in this *Accepted Manuscript* or any consequences arising from the use of any information it contains.



Journal Name

ARTICLE

Understanding the Hydrogen Bonds in Ionic Liquids and their Roles in Properties and Reactions

Received 00th January 20xx,
Accepted 00th January 20xx

DOI: 10.1039/x0xx00000x

www.rsc.org/

KunDong,^a SuojiangZhang^{a,*} and Jianji Wang^{b,*}

Ionic liquids (ILs) show the great potential applications in chemical industries. To understand ILs, their molecular details have been investigated extensively. Intuitively, the electrostatic force is solely important for ILs. However, experiments and calculations have provided strong evidences about the existence of H-bonds in ILs and their roles in the properties and applications of ILs. As the structural directing contributor, H-bonds are responsible for ionic pairing, stacking and self-assembling. The geometric structure, interaction energy and electronic configuration in the ion-pairs of imidazolium-based ILs and protic ionic liquids (PILs) show great number of differences from the conventional H-bonds. In particular, the cooperation with the electrostatic, dispersion and π interactions embodies the physical nature of H-bond in ILs, which anomalously influences the properties and leads to the decrease of melting points and viscosities, and fluidize the ILs. Using ILs as catalysts and solvents, many reactions can be activated by the presence of H-bond to reduce the reaction barrier and stabilize the transition state. In the dissolution of lignocellulosic biomass by ILs, the H-bond exhibit most important role in disrupting the H-bonding network of cellulose and controlling microscopic ordering into domains. In this article, a critical review is presented for the structural features of H-bond in ILs and PILs, the correlation between H-bonds and the properties of ILs, and the roles of H-bonds in typical reactions.



Dr. Kun Dong received his master degree from the University of Petroleum, Beijing in 2004. After that, he worked as a researcher at Institute of Process Engineering (IPE), Chinese Academy of Sciences (CAS). In 2013, he received his Ph.D. degree from the Institute, now he is an associate Professor at IPE. His researches have focused on exploration of structures and properties of ILs by computational simulations and the molecular design of task-special ILs for the chemical processes.

than 5000 citations have been reported. Six monographs have been written or edited, and more than 60 patents have been authorized. He won the Second Class Prize of National Natural Science Award of China in 2010.



Prof. Suojiang Zhang is the director general of IPE, CAS. He received his Ph.D. degree from Zhejiang University in 1994. He mainly engages in the researches of ILs and green processes, including molecular design, large-scale preparation and green processes of ILs. Until now, a total of 360 SCI papers have been published in academic journals, and more

Prof. Jianji Wang received his Msc. at Wuhan University (China), and Ph.D. at Yokohama National University (Japan). He worked as a research fellow at University College London (1987-1989) and University of Surrey (1992-1993). He became a professor of physical Chemistry at HNU in 1994. His current research interests are centered in structure – property relationship of ionic liquids and their applications in green separation and biomass processing. He has authored around 300 scientific publications in peer-reviewed journals, and serves as the editorial board member of Journal of Chemical Thermodynamics.



1. Introduction

Possessing many favourable physicochemical properties such as low melting point, wide liquid range, negligible vapour pressure, high thermal stability, excellent solubility and tunable hydrophobicity and acidity, room temperature ionic liquids (RTILs) have attracted widespread academic and industrial interests and achieved quite a few successes in past two decades.¹⁻³ Each breakthrough, such as dissolving cellulose⁴, liquid mirror in space telescope^{5,6}, and catalyst

^a State Key Laboratory of Multiphase Complex System, Institute of Process Engineering, Chinese Academy of Sciences, Beijing 100190, P. R. China. E-mail: sjzhang@ipe.ac.cn; Fax: +86-10-82627080; Tel: +86-10-82627080.

^b Collaborative Innovation Center of Henan Province for Green Manufacturing of Fine Chemicals, School of Chemistry and Chemical Engineering, Key Laboratory of Green Chemical Media and Reactions, Ministry of Education, Henan Normal University, Xinxiang, Henan 453007, P. R. China. E-mail: jwang@htu.cn.

in CO₂ electro-reduction⁷, is pregnant with new technology. Since the air-stable ILs containing the anions [PF₆]⁻, [BF₄]⁻, and [NTf₂]⁻ were reported in the 1990s,^{8,9} the RTILs have been applied into various aspects, such as CO₂ capture¹⁰⁻¹³, extraction/separation¹⁴⁻¹⁶, synthesis and catalytic reaction², electrochemical and metallurgy¹⁷⁻²¹, soft material²²⁻²⁴, and biosystems^{25,26} and more others, and some results were quite encouraging. Recent developments have prompted ILs to be filled in confined environments, such as carbon nanotube and graphene, thus leading to many new applications²⁷⁻³⁰.

The RTILs have been honoured as the “designed solvents” by combing different anions and cations to lead to their diversity, and the reported possible combination reaches to about a million³¹. Thus, the prediction of properties becomes very critical in applications of the ILs. An important employment is to build the quantitative structures and properties relationship (QSPR) to predict the properties of the ILs.³ In QSPR studies, the structures are fundamentally important, however, the structures of ILs are more complicated than that of the classic salts. Besides the large sizes and asymmetric shapes, many properties are closely relevant with the non-covalent interactions, which are of great importance for understanding ILs and their behaviours. Intuitively, it seems that the strong electrostatic interaction (Coulomb force) is only important in the ILs. However, the low melting points possessed by most of ILs defy this consideration, so the “pure ionization” model is too simplistic to predict the properties of ILs correctly.

By dissociation of total interaction energy, Kirchner et al.³² found that the dispersion force in 1,3-dimethylimidazolium chloride ([C₁C₁im]Cl) ion-pair is notably stronger than that in NaCl pair. The Coulomb force is only 70% of the total energy, which indicates that the weaker interactions cannot be ignored.³³ Especially, H-bond is considered to be critical for structure and interaction modes of ILs. X-ray diffraction, IR and NMR spectroscopy have provided the strong evidences for the existence of H-bond in ILs at both solid and liquid states. In imidazolium-based ILs, the H-bond is characterized by the shorter C–H...anion distances, red shift of C–H stretching and downfield shift of C–H proton chemical shifts.³⁴⁻³⁷ At the same time, a large number of theoretical calculations have also been performed to investigate the H-bonding interactions. Dong et al. investigated the interactions in imidazolium tetrafluoroborate salt ([C₂C₁im][BF₄]) and hexafluorophosphate salt ([C₄C₁im][PF₆]) by DFT calculations and found that there exist C–H...F H-bonds between cations and anions.³⁸ Furthermore, they reviewed the structural characteristics of H-bonds in the different ILs, relationship with the properties and roles in applications in recent publications.³⁹ Seddon et al.⁴⁰ investigated the interactions of ions in the solid state for a series of representative [C_nC₁im][PF₆] salts. By examining the distance between donor atom (C–H) and acceptor atom (F), it was found that there are specific directional H-bonds to [PF₆]⁻ anions or the format ion of interstitial voids. Recently, Ludwig et al.^{41,42} focused their attentions on characterization of H-bonds in ILs by low-frequency spectroscopy combined with DFT calculations and

molecular dynamics (MD) simulations. They found that the H-bonds in imidazolium-based ILs perturb the Coulomb forces to deviate from charge symmetry, finally result in the decreased viscosities and enhanced fluidization of the ILs. Besides viscosities, the melting point and enthalpy of vaporization also correlate with the H-bonds^{43,44}.

In the imidazolium-based salts, the hydrogen atoms on imidazolium ring are mainly involved in the formation of H-bonds. Experimental investigations indicate that the hydrogen atom at C²-H is more acidic than that at C^{4/5}-H, which suggests the formation of stronger H-bonds between donor C²-H and anionic acceptor.^{45,46} However, there is also experimental evidence to support the binding into transition metals at C^{4/5}-H.⁴⁷ Compared with imidazolium salts, the N-alkylpyridinium and N-alkylpiperidinium-based ILs show weaker H-bonding interactions between the hydrogen atoms of N–CH₃ and the electron rich center of anion.⁴⁸ For tetraalkylammonium or tetraalkylphosphonium-based ILs, the α-hydrogen is acidic and involves in forming C–H...anion H-bonds. However, when the alkyls are replaced by hydrogen atoms, the ILs, such as ethylammonium nitrate ([EtNH₃][NO₃]), belong to PILs, in which the strong N–H...anion H-bonds (N is nitrogen atom) form between donor and acceptor.^{49,50} The PILs are an important subgroup of ILs produced by a combination of equimolar amounts of Brønsted acid and base. These PILs have been applied in chemical reactions as catalyst and in electrochemical processes as electrolyte, especially in fuel cell and lithium-ion battery.⁵¹ The key property that distinguishes PILs from other ILs is the proton transfer, which leads to the presence of proton-donor and -acceptor sites, and then the formation of the H-bonds. Experiments and calculations have proved that there are stronger H-bonds in PILs.⁵²⁻⁵⁵

In practice, ILs are often mixed with molecular compounds or solid materials to improve their properties, most commonly with water to decrease viscosity and increase conductivity of ILs.⁵⁶ From measurement of ATR and transmission IR spectroscopy, Welton et al. found that in the aqueous ILs solution, the water molecules exist in symmetric 1:2 type H-bonded complexes anion...HOH...anion at the concentration range investigated.⁵⁷ In PILs, water can disrupt the H-bonding network to form the nano-clusters.^{55,58} With the formation of H-bonds, the charge is transferred from anion to cation directly to result in the non-integer charges (0.6-0.8e)⁵⁹. The resulting electron delocalization arises as a consequence of the constituent ions in the ion-pair and local nano-structural organization.^{60,61} In particular, the PILs show A⁺...H...B⁻ H-bonding structure in proton transfer, and the proton is dissociated from cation to anion.⁶²

In applications of ILs, H-bond also plays important roles. Especially in some reactions involving ILs as catalysts and solvents, H-bonds can stabilize transition state (TS) to enhance the conversion.^{63,64} H-bonds can be also used to control supramolecular aggregation, self-assembly, and microscopic ordering into domains, from the generation of nanoscale domains or micelles to the formation of structured liquid crystal phases in crystal engineering. So far, it is

clear that H-bond is ubiquitous in ILs and in their mixtures, and becomes the key structural factor for the QSPR. However, it has been argued that the H-bond is not essential for some ILs with cations of pyridinium and phosphonium and anions of $[\text{PF}_6]^-$ and antimony hexachloride ($[\text{SbCl}_6]^-$). In fact, the only reason is that the H-bonds in these ILs are weaker and the corresponding signatures in the spectra may be resulted from other contributions.^{65,66} Up to date, the results about the H-bonds in ILs have emerged in large numbers, but to our knowledge, a review on the uniqueness of H-bonds and their roles in reactions has not presented. In this work, the structural features of H-bond in common ILs and PILs were discussed based on the results of experiments and calculations, then H-bonds are correlated with the properties of ILs, and finally the roles of H-bonds in typical reactions are reviewed.

2. H-bonds in imidazolium-based ILs

2.1 Resonance structure of imidazolium cation

The imidazolium ring is usually assumed to be aromatic and the electrons delocalize on the ring. However, a question “how delocalized are the electrons?” is not well answered. Fig. 1 shows the resonance structures of the imidazolium cation that exhibit significant π -electron delocalisation.⁶⁷ The six π electrons distribute over five p orbitals. If the six π electrons are equally distributed over the ring atoms, each would have 1.2 π electrons. The occupancy of the formally empty C^2 p orbital can therefore be used to give an indication of the extent of delocalization.⁶⁸ Using this criteria the $[\text{C}_4\text{C}_1\text{im}]^+$ cation exhibits a very high level of delocalization of 80.3%.

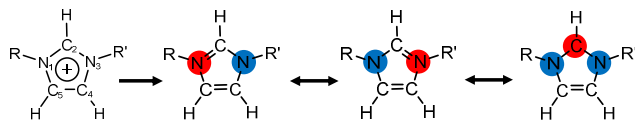


Fig. 1 Resonance structures of imidazolium cation. Red colour notes the area of positive charges and blue colour notes the area of negative charges.

However, Natural bond orbital (NBO) analysis indicates that four electrons are localized into $\text{N}^1\text{-C}^2\text{-N}^3$ atoms to form three-center four-electron configuration and the other two electrons enter into a p -type antibonding orbital on the double bond between C^4 and C^5 atoms. The electronegativity of the ring atoms ensures that electrons cannot equally distribute along the ring. The σ induction usually “pushes” more electrons onto the more electronegative nitrogen atoms, but significant occupation of the $\text{C}^2\text{-N}^1$ π^* bond (0.54e) “pulls” electrons away from the nitrogen atoms, finally the σ induction and π delocalization result in a “push–pull” effects on electrons. Hence, any addition of electrons to this system may increase antibonding and destabilization of the electron.⁶⁹ The general feature of charge distribution on the cation is that the positive charges are located on the peripheral hydrogen atoms and the negative charges are located on the nitrogen atoms, while the $\text{C}^{4/5}$ carbon atoms remain essentially neutral. For the side chains,

the carbon atoms are negatively charged, except for those adjacent to the ring, but summing the positive charges of hydrogen atoms into the heavy carbon atoms leaves roughly neutral methyl or methylene group. In chemical reactions, the acidity of H atoms on the ring, especially the most acidic $\text{C}^2\text{-H}$ hydrogen are particular interesting.^{70,71} However, Bühl et al. found that hydrogen atoms on $\text{C}^{4/5}\text{-H}$ and $\text{C}^2\text{-H}$ of the cation carry similar charges on the cation, and there is no more acidic hydrogen on C^2 atom.⁷² The result is in agreement with experimental observations⁷³ when the charges of hydrogen atoms are summed into heavy atoms for $[\text{C}_4\text{C}_1\text{im}]^+$ and the total charges are $q(\text{C}^2\text{-H})=+0.536$, $q(\text{C}^4\text{-H})=+0.239$ and $q(\text{C}^5\text{-H})=+0.242$, respectively. Thus the relative acidity should not be associated with the H atoms alone, but with the charge on the “C–H” moiety.

2.2 H-bonds in the ion-pairs

Although the ILs are composed of cations and anions, the existence of neutral ion-pairs is arguable. It is reported from MD simulations that no long-lived ion-pairs has been found and the vast majority of ions do not travel together as neutral ion-pairs, which has been used to explain the failure of Nernst-Einstein approximation.^{74,75} Nevertheless, the interactions between anion and cation are substantially important as the threshold to understand the behaviour and property of ILs.^{32,76}

2.2.1 Geometric structure

Up to date, the definition of H-bond has been extended.⁷⁷⁻⁸⁰ For the $\text{X-H}\cdots\text{Y}$ model, the acceptor Y needs not to be a base with a lone-pair electron, but is an area where there is a buildup of electron density. Moreover, the donor X is now widely recognized to be less electronegative atoms such as S, C, Se, Si or a halogen. The resonance assisted H-bonds, $\text{X-H}\cdots\pi$, $\pi\cdots\text{H}\cdots\pi$ and $\text{H}\cdots\text{e}\cdots\text{H}$ have been reported. In addition, the H-bonds formed between a neutral molecule and a charged ion, such as $\text{NH}_4^+\cdots\text{NH}_3$ and $\text{NH}_4^+\cdots\text{H}_2\text{O}$ have been termed as “strong ionic H-bond”.⁸¹ However, the H-bonds in ILs formed between both charged ions are not the case, and the H-bonds have not been examined in details and the interactions have simply been explained as ionic. To differentiate the H-bonds in ILs from the already well established H-bonds, Hunt et al.⁸² referred to the H-bond as “the doubly ionic H-bond”.

Hunt et al.⁸³ and Tsuzuki et al.⁸⁴ investigated the geometric structures of the typical ion-pairs by DFT calculations. For example in 1-ethyl-3-methylimidazolium trifluoroacetate ($[\text{C}_2\text{C}_1\text{im}][\text{CF}_3\text{CO}_2]$), the anion $[\text{CF}_3\text{CO}_2]^-$ favours to locate close to the $\text{C}^2\text{-H}$ group of cation to form $\text{C-H}\cdots\text{O}$ H-bonds with the $\text{C}^2\text{-H}$. Similarly in 1-ethyl-3-methylimidazolium triflate ($[\text{C}_2\text{C}_1\text{im}][\text{CF}_3\text{SO}_3]$), the $-\text{SO}_3$ group has a closer contact with the $\text{C}_2\text{-H}$ group to form $\text{C-H}\cdots\text{O}$ H-bonds. In the 1-ethyl-3-methylimidazolium bis(trifluoromethylsulfonyl)imide ($[\text{C}_2\text{C}_1\text{im}][\text{NTf}_2]$) ion-pair, there are H-bonds between the $\text{C}_2\text{-H}$ group of cation and the N atom or $-\text{SO}_2$ group of the anion, and the $-\text{SO}_2$ group is above the imidazolium ring. But in $[\text{C}_2\text{C}_1\text{im}][\text{BF}_4]$, the anion

$[\text{BF}_4]^-$ can locate above or below the imidazolium ring. Thus, the H-bond is very system dependent in different ILs, and the possible reason is that H-bond is not a binary on-off phenomenon but occurs in a graduated scale which makes it difficult to quantify and demark the H-bond.³⁹

For the same cation, the H-bonds can be classified by increasing complexity of anions from the simplest single atom halide anions, small diatomic anions such as $[\text{HS}]^-$ and $[\text{CN}]^-$, and the highly symmetric multi-atom $[\text{BF}_4]^-$ and $[\text{PF}_6]^-$ anions to the less symmetric $[\text{NTf}_2]^-$ and $[\text{CF}_3\text{SO}_3]^-$ anions.^{39, 84} Usually, multiple H-bonds can form in an ion-pair and exhibit bifurcated and chelated structure. Fig. 2 shows the representative ion-pairs and forming H-bonds (dashed lines). It can be seen that there are two C-H \cdots Cl H-bonds in $[\text{C}_2\text{C}_1\text{im}]\text{Cl}$ (Fig. 2A) and four C-H \cdots F H-bonds in $[\text{C}_2\text{C}_1\text{im}][\text{BF}_4]$ (Fig. 2B) that show bifurcated and chelated structure. For the anions $[\text{N}(\text{CN})_2]^-$, $[\text{OAc}]^-$, $[\text{CF}_3\text{SO}_3]^-$ and $[\text{HSO}_4]^-$, etc. with the stronger H-bonding acceptors, one anion can “occupy” multiple positions around the same cation to form the multiple but distant (not adjacent) H-bonds. For example in $[\text{C}_2\text{C}_1\text{im}][\text{OAc}]^-$, the $-\text{COO}$ group orients the front position of the cation to form four C-H \cdots O H-bonds that show the bifurcated and chelated structure (Fig. 2C). For the complex anions including linker groups/atoms and internal torsional motions, e.g. $[\text{NTf}_2]^-$ with more than one type of H-bond acceptor (e.g. O and N within $[\text{NTf}_2]^-$), there are different types of H-bonds as shown in Fig. 2D, which have both an electron rich central N atom and pendant groups, containing O and N atoms, respectively. Normally, the O-atoms are assumed to dominate the H-bonding interactions, but all the electronegative atoms are available in forming the H-bonds.

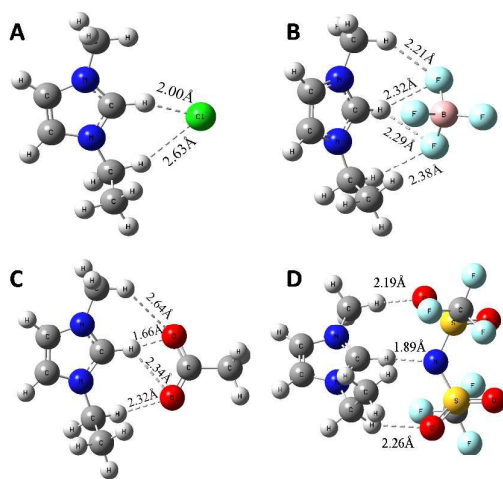


Fig. 2 Representative ion-pairs and the H-bonds (dashed lines). (A) $[\text{C}_2\text{C}_1\text{im}]\text{Cl}$ with C-H \cdots Cl H-bonds. (B) $[\text{C}_2\text{C}_1\text{im}]\text{Br}$ with C-H \cdots Br H-bonds. (C) $[\text{C}_2\text{C}_1\text{im}][\text{BF}_4]$ with C-H \cdots F H-bonds. (D) $[\text{C}_2\text{C}_1\text{im}][\text{NTf}_2]$ with C-H \cdots N and C-H \cdots O H-bonds and the distances of H \cdots Y are shown in angstrom.^{33, 38, 83}

2.2.2 Interaction energy

The total interaction energy (ΔE) is a measurement for stability of an ion-pair. The calculated ΔE values for the $[\text{C}_2\text{C}_1\text{im}][\text{CF}_3\text{CO}_2]^-$, $[\text{C}_2\text{C}_1\text{im}][\text{BF}_4]^-$, $[\text{C}_2\text{C}_1\text{im}][\text{CF}_3\text{SO}_3]^-$, $[\text{C}_2\text{C}_1\text{im}][\text{NTf}_2]^-$ and $[\text{C}_2\text{C}_1\text{im}][\text{PF}_6]^-$ ion-pairs at the MP2/6-311* level are -375.72, -356.48, -345.60, -329.70, and -328.03 kJ/mol, respectively,^{32, 84} which indicates the stabilities of the ion-pairs follow the order: $[\text{CF}_3\text{CO}_2]^- > [\text{BF}_4]^- > [\text{CF}_3\text{SO}_3]^- > [\text{NTf}_2]^- > [\text{PF}_6]^-$. It seems that the energies are not closely relevant to the sizes and symmetries of these anions. However, the charge distribution is likely responsible for this order. For example, negative charge on $-\text{CO}_2$ group of $[\text{CF}_3\text{CO}_2]^-$ is higher than that on $-\text{SO}_3$ group of $[\text{CF}_3\text{SO}_3]^-$, which results in the larger ΔE (more negative) in $[\text{C}_2\text{C}_1\text{im}][\text{CF}_3\text{CO}_2]^-$ than in $[\text{C}_2\text{C}_1\text{im}][\text{CF}_3\text{SO}_3]^-$. It is found in the ion-pairs with the large ΔE values that the anion usually prefers to have close contact with $\text{C}^2\text{-H}$ of the imidazolium cation to form the $\text{C}^2\text{-H}\cdots$ anion H-bonding configurations. For example $[\text{C}_2\text{C}_1\text{im}][\text{CF}_3\text{CO}_2]^-$ and $[\text{C}_2\text{C}_1\text{im}][\text{CF}_3\text{SO}_3]^-$ exhibit the $\text{C}^2\text{-H}\cdots\text{O}$ H-bonds. However, some configurations in which anions interacts above/below the imidazolium ring are also stable and have nearly equal ΔE values with the H-bonding configurations. For the $[\text{C}_2\text{C}_1\text{im}][\text{CF}_3\text{CO}_2]^-$, the ΔE value of H-bonding configuration and the above/below configuration are, respectively, -375.72 kJ/mol - 354.38 kJ/mol, and the difference is only 21.34 kJ/mol. For the ion-pair $[\text{C}_2\text{C}_1\text{im}][\text{BF}_4]^-$, the ΔE value of above/below configuration is 323.42 kJ/mol and the difference from that of the H-bonding configuration is 33.06 kJ/mol. Molecular dynamic (MD) simulation and neutron diffraction have also provided evidences that the anion prefers to locate above/below the imidazolium ring.⁸⁵⁻⁸⁸ The above/below configurations may be energetically relevant to the π electrons that delocalize on the imidazolium ring and the π interaction decreases the ΔE value and makes the configurations stable.

The decomposition of interaction energy is an approach to estimate the contribution of the different energies. Symmetry adapted perturbation theory (SAPT) is a popular method for accurately calculating the interaction energies of a dimer. In SAPT, the interaction energy is expressed as a sum of perturbative corrections in the intermolecular interaction operator V .⁸⁹ In order to allow a better insight into the nature of interaction mechanism each of the correction is classified to describe one of the four fundamental interactions: electrostatic, induction, dispersion, or exchange. Such insight is helpful in understanding of the trends in spectroscopic and scattering experiments. Based on SAPT decomposition, Zahn et al.³² compared the component energies of the ion-pair $[\text{C}_1\text{C}_1\text{im}]\text{Cl}$ and with the traditional NaCl and found that main contribution of the interaction energy stems from the electrostatic interaction for the both ion-pairs. However the dispersion term is not negligible in $[\text{C}_1\text{C}_1\text{im}]\text{Cl}$ and the induction term in magnitude is comparable to that in NaCl. An observation concerning the minima of the NaCl at the equilibrium distance features the minima exactly for all curves exactly, however, to our surprisingly, this is not the case for the $[\text{C}_1\text{C}_1\text{im}]\text{Cl}$ pairs. This means that the equilibrium distance is not exclusively determined by the electrostatic interaction. ILs are not as ionic as one may naively imagine and different contributions

compensate each other partly, resulting in a shallow potential energy curve. Consequently, the system is highly flexible and liquid-like and it is also able to adjust easily to different situations.

2.2.3 Charge distribution

Sum of the charges of cation and anion should be a formal charge of $\pm 1e$ for $[A]^+[B]^-$ salts. However, it is found from NBO analysis that the overall positive charge on $[C_2C_1im]^+$ cation in $[C_2C_1im][BF_4]$ is $+0.953e$, which indicates the electrons can transfer from anion to cation. The reduction of charge suggests the necessary for the properly description of charges of the salts.⁹⁰⁻⁹² The partial charges on the atoms surrounding the H-bond are expected to have a more significant effect than the partial charges on the periphery of the molecules. Fig. 3 presents an electron density difference map of $[C_2C_1im]Cl$ ion-pair, and it is clear that the electron density of Cl^- anion is polarized to move toward the cation, then leading to the increase of density in the $C-H\cdots Cl$ region. Specifically, the decrease in electron density of the H atom indicates the more positive charge distribution. Though the electron density around the C^2 atom increases, the partial charge of the atom is constantly positive. The charge distribution of H-bond shows $X^{\delta+}-H^{\delta+}\cdots Y^{\delta-}$ distribution in the ion-pair that is different from the $X^{\delta-}-H^{\delta+}\cdots Y^{\delta-}$ distribution in the conventional H-bonds. This kind of “non-local” effect was discussed more commonly in reference to blue shifted frequency.⁹³

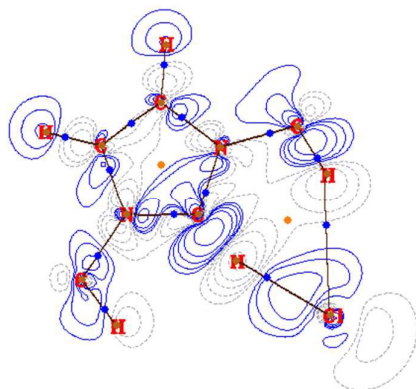


Fig. 3 Contour map of the electron density difference obtained at the MP2/6-311+G(d,p) level. The contour map is projected on the imidazolium ring plane. The blue solid lines show the increment of electron density and gray dashed lines show the decrease of the electron density.

Similar charge distributions have been reported recently in the ILs $[C_2C_1im][NTf_2]$, $[C_2C_1im][OAc]$ and quaternary ammonium N-methylacetamide ($[NC_4][NMA]$). Though positive charges on the hydrogen atoms and the negative charges on the acceptor Y atoms are increased, the impact on the donor X atoms of the cation is less predictable.^{94, 95} According to this charge scaling effect,^{96, 97} the total charge of a univalent ion should be located between 0.6 and 0.8 e. Krossing et al.⁵⁹ investigated the charges of 1-methyl-3-methylimidazolium methylsulfate ($[C_1C_1im][C_1SO_4]$) ion-pair by high

resolution X-ray diffraction (XRD) combined with the atom in molecule (AIM) calculation. The corresponding ionic net charges $q^{+/-}$ (exp.) = 0.90e and $q^{+/-}$ (cal.) = 0.87e and they suggested that the efficient charge transfer along the bond paths of the H-bonds between the imidazolium ring and the anion was considered as the origin of these reduced charges. In the $[C_1C_1im]Cl$, a charge of -0.82 upon extrapolation to infinite cluster size was reported for the chloride ion. However, Schmidt et al.⁹⁰ calculated an even smaller charge $q^{+/-}$ = 0.63 e charge for the ions of $[C_1C_1im][Cl]$ in the bulk phase. In many MD simulations, the charged scaling of 0.9 was used in IL-water interfaces, while the scaling by $\epsilon^{-0.5}$ was used in high- and low-dielectric media, ion-solvent systems and ionic groups in proteins,^{69, 90-92, 98, 99} where ϵ is the electronic component or high-frequency limit of the relative permittivity.

2.2.4 Features described by AIM, MO and NBO

AIM, molecular orbital (MO) and NBO analyses provide electronic description to understand the H-bonds in ILs. Usually, the densities at basin critical point (BCP), ρ_{BCP} of a H-bond is 0.002-0.035 a.u. and Laplace values of the density, $\nabla^2\rho_{BCP}$ are 0.024-0.139 a.u. in the AIM analysis.¹⁰⁰ In the $[C_1C_1im]Cl$ ion-pair, the ρ_{BCP} = 0.0453 a.u. for the $C^2-H\cdots Cl$ H-bond and ρ_{BCP} = 0.014 a.u. for the $C^6-H\cdots Cl$ H-bond. The corresponding values of $\nabla^2\rho_{BCP}$ are 0.072 and 0.037 a.u., respectively. In the $[C_4C_1im]X$ (where $X=[BF_4]^-$, $[PF_6]^-$) ion-pairs with $C-H\cdots F$ H-bonds, the ρ_{BCP} values are within 0.016-0.019 a.u. In the case of $X=[H_2PO_4]^-$, $[HSO_4]^-$, $[CF_3CO_2]^-$ anions with $C-H\cdots O$ H-bonds, the values of ρ_{BCP} are 0.046-0.050 a.u. When experimental density is correlated with the basicity of ILs (β -value, H-bond acceptor), the basicity of ILs is enhanced with the decrease of the H-bonding strength.¹⁰¹

MOs, especially frontier MOs (FMOs) can be used to interpret the electronic interaction involved in the H-bonds. Fig. 4A shows FMO energy-level diagram of the $[C_1C_1im]Cl$ ion-pair. It is found that the highest occupied MO (HOMO) of Cl^- anion is the p orbitals (pAO) and lowest unoccupied MO (LUMO) of the imidazolium cation consists of high-energy σ^*_{C-H} orbitals. The interaction domains can be roughly broken down into Coulomb and orbital components. The strong electrostatic attraction (Coulomb component) induces the decrease of orbital energies of the cation and the increase of orbital energies of the anion, so that orbital overlap is facilitated. In the process that Cl^- anion approaches cation to form ion-pair in plane (orbital component), the LUMOs of the ion-pair are very similar to LUMOs of the isolated cation orbitals and the HOMO is one of the three pAO s of Cl^- anion, which indicates that covalent interaction is minimal. However, the deeper HOMOs (insertion in Fig. 4A) formed by an empty C^2-H σ^* -bond orbital and a filled pAO of the Cl^- show σ symmetry, in which the H atomic orbital is in plane with Cl^- anion and polarized toward the anion. A clear contribution from the C^2 pAO s is also found indicate that the C-H unit, rather than the H atom, is important for the efficient orbital overlap and the formation of the H-bond. In the ion-pairs where the Cl^- anion lies above or below the imidazolium ring, these orbitals exhibit a

bonding and antibonding couple composed of an interaction between the Cl^- pAOs and the cation HOMO. Fig. 4B shows NBO analysis. In order to make a comparison, a neutral imidazole-2-ylidene is also considered. The pAOs of Cl^- anion are used as a reference level to compare with the cation. It can be seen that the NBOs are stabilized on moving from the neutral to the cation species. However, in the presence of the anion, the bonding C–H σ

NBOs of the cation are destabilized relative to the isolated cation and unexpectedly have the energies very similar to those found in the neutral imidazole-2-ylidene (dotted blue line). The antibonding C–H σ^* NBOs are more sensitive to the charge and drop below the neutral C–H σ^* NBOs. The C–H σ^* NBOs also interact weakly with one of the Cl^- 3p lone pairs to form a bonding-antibonding pair (interaction shown in red). There is a slight stabilization of the Cl lone pair NBO and significant destabilisation of the C–H σ^* NBO.

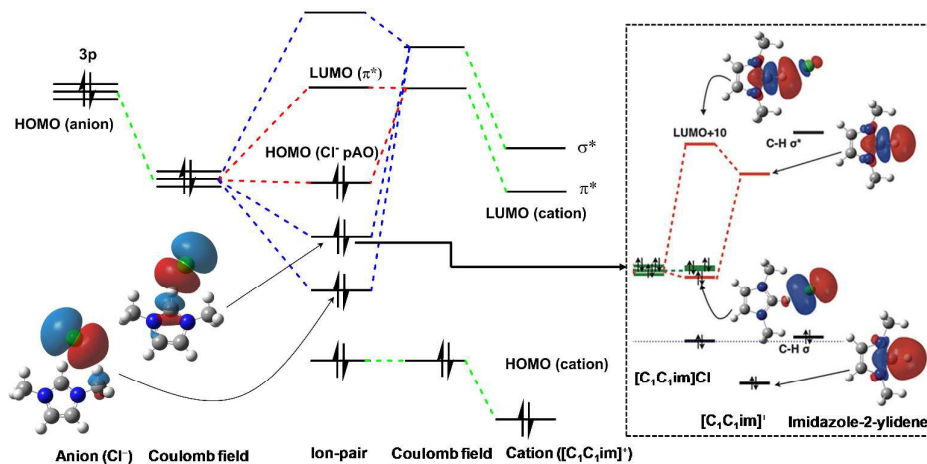


Fig. 4 MO and NBO energy-level diagram for $[\text{C}_1\text{C}_1\text{im}]\text{Cl}$ ion-pair. (A) FMO interactions.⁶⁹ The dotted blue and red lines show the orbital interactions, and two orbitals with σ symmetry are shown. (B) NBO analysis, the dotted blue lines show the generalized reference for the neutral σ -bonding NBO energies. NBOs of Cl^- anion are shown in green and NBOs of cation are shown in red.

It has been demonstrated that the H-bonding strength of the $n_Y \rightarrow \sigma_{X-H}^*$ donor-acceptor follows the same trend with NBO delocalization energies, $E_{n \rightarrow \sigma^*}^{(2)}$ expressed by Equ. 1¹⁰².

$$E_{n \rightarrow \sigma^*}^{(2)} \cong -2 \frac{\langle n | \hat{F} | \sigma^* \rangle^2}{E_{\sigma^*} - E_n} \quad (1)$$

Here $n\sigma^*$ is the Fock matrix element, which is approximately proportional to the PNBO overlap $S_{n \rightarrow \sigma^*}$ and $E_{\sigma^*} - E_n$ is the orbital energy difference between the σ^* and n NBOs.

Table 1 lists the $E_{n \rightarrow \sigma^*}^{(2)}$ values of some typical ion-pairs and H-bonds formed in the ion-pairs. For the sake of comparison, the $E_{n \rightarrow \sigma^*}^{(2)}$ values of neutral $[\text{NH}_3][\text{H}_2\text{O}]$ and ionic $[\text{NH}_4]^+[\text{H}_2\text{O}]$ and $[\text{NH}_3][\text{OH}]^-$ are also listed.^{81, 103} It can be seen that the $E_{n \rightarrow \sigma^*}^{(2)}$ values for the neutral $[\text{NH}_3][\text{H}_2\text{O}]$ is 13 kJ/mol, which is far less than that of the ionic $[\text{NH}_4]^+[\text{H}_2\text{O}]$ (126 kJ/mol) and $[\text{NH}_3][\text{OH}]^-$ (130 kJ/mol). The result indicates that the strength of H-bond increases when one end of the H-bonding dimer is partially charged. Moreover, it can be seen from Table 1 that for the IIs whose two ends are partially charged, the $E_{n \rightarrow \sigma^*}^{(2)}$ values are larger than that of ionic H-bonds. For the imidazolium-based ion-pairs with $[\text{BF}_4]^-$ and $[\text{PF}_6]^-$ anions, the $E_{n \rightarrow \sigma^*}^{(2)}$ values are 50-60 kJ/mol,

indicating that the C–H \cdots F H-bond is weak in strength. On the other hand, for the imidazolium-based ion-pair with Cl^- and $[\text{NO}_3]^-$ anions, the $E_{n \rightarrow \sigma^*}^{(2)}$ values are 110-180 kJ/mol, suggesting the stronger C–H \cdots Cl and C–H \cdots O H-bonding strengths^{33, 102}. For shown $[\text{EtNH}_3][\text{NO}_3]$, $[\text{PropNH}_3][\text{NO}_3]$ and $[\text{Me}_3\text{NH}][\text{Cl}]$ ion-pairs of the PILs in Table 1, the $E_{n \rightarrow \sigma^*}^{(2)}$ values are as large as 250-320 kJ/mol, indicating the strongest N–H \cdots O H-bonds.^{54, 102} In particular, the $E_{n \rightarrow \sigma^*}^{(2)}$ value is possible to exceed the overall interaction energy. For less extreme case, for example $E_{n \rightarrow \sigma^*}^{(2)}$ value of $[\text{Me}_3\text{NH}][\text{Cl}]$ ion-pair is 523 kJ/mol that is larger than the interaction energy of 485 kJ/mol. Thus, the covalent part of the H-bond is highly stabilizing, while other interactions within the complex must be destabilizing. The substantial increase in charge transfer can decrease the energy of the cationic empty X–H σ^* orbital and raise the energy of anionic Y lone pair, leading to decrease of the energy gap and the increase of the $E_{n \rightarrow \sigma^*}^{(2)}$ value.

Table 1. Values of $E_{n \rightarrow \sigma^*}^{(2)}$ and H-bonds for the typical ion-pairs

	$E_{n \rightarrow \sigma^*}^{(2)}$ (kJ/mol)	H-bonds	Ref.
$[\text{C}_1\text{C}_1\text{im}]\text{Cl}$	173	C–H \cdots Cl	82
$[\text{C}_1\text{C}_1\text{im}][\text{BF}_4]$	50	C–H \cdots F	104
$[\text{C}_1\text{C}_1\text{im}][\text{NTf}_2]$	119	C–H \cdots N, C–H \cdots F	104
$[\text{C}_2\text{C}_1\text{im}]\text{Cl}$	179	C–H \cdots Cl	105

[C ₂ C ₁ im][BF ₄]	56	C-H...F	33
[C ₄ C ₁ im][PF ₆]	55	C-H...F	33
[C ₄ C ₁ im][NO ₃]	111	C-H...O	102
[EtNH ₃][NO ₃]	320	N-H...O	54
[PropNH ₃][NO ₃]	250	N-H...O	102
[Me ₃ NH]Cl	523	N-H...Cl	82
[NH ₃][H ₂ O]	13	N-H...O	103
[NH ₄] ⁺ [H ₂ O]	126	N-H...O	81, 103
[NH ₃][HO] ⁻	130	N-H...O	81, 103

2.2.5 Cooperation with electrostatic, dispersion and π interactions.

The total ΔE values for a conventional neutral H-bond are 8–65 kJ/mol, and when one component is ionic, the energies are increased to 40 – 190 kJ/mol⁸¹. When both components are ionic, the energies are larger than 300 kJ/mol as discussed above. Obviously, the electrostatic interaction has a substantial contribution to the total energy. The dispersion force is also proven to play important roles in the structures of ILs.¹⁰⁶ In addition, π -type interactions have been observed in crystals, liquids and mixtures of imidazolium-based ILs.^{107–110} Thus, the total energy is the result of a balance between strong and weak interactions, and the H-bond discussed is actually cooperative with electrostatic, dispersion and π interactions.

From *ab initio* calculations, Izgorodina et al.¹¹¹ reported the cooperation of H-bonding interaction with electrostatic and dispersion interactions by comparing the geometries, composite energies and net charge transfer (NCT) of neutral molecule-molecule dimer (H₃C-H...F-H), with those of molecule-ion dimer (H₃C-H...F⁻ and H₃C-H...Cl⁻) and ion-ion dimer ([C₂C₁im]Cl ion-pairs). The results are listed in Table 2. It is found that dispersion force is dominant in H₃C-H...F-H dimer, but has the negligible effect on the geometry of the H-bond (ΔR_{C-H} 0.000 Å and $\angle C-H...F$ 180°). For the H₃C-H...F⁻ and H₃C-H...Cl⁻ dimers, induce, dispersion and electrostatic forces are almost equivalent and jointly have more effect on the geometry (ΔR_{C-H} 0.023 Å for H₃C-H...F⁻ and ΔR_{C-H}

0.015 Å for H₃C-H...Cl⁻). For the [C₂C₁im]Cl ion-pairs, electrostatic force is dominant, for example, the electrostatic energy of ion-pair1 is 77% of the total energy and the dispersion force is also increased, which makes substantial effect on the geometry.

The C-H bonds are longer and the angles are bent significantly in the dimers (ΔR_{C-H} 0.046, 0.024, and 0.025 Å and $\angle C-H...Cl$ 159, 148, and 150° for ion-pair1, 2 and 3, respectively). Larger net charge transfer (NCT) can be observed in Table2 for the [C₂C₁im]Cl ion-pairs. As suggested by MacFarlane et al.¹¹¹, the cooperation causes some differences and the ionic conformers can not necessarily be thought of as the traditional H-bond because the electrostatic force and dispersion contributions are considerably larger than those in the conventional H-bonded systems.

Fumino et al.¹⁰⁶ described the balance between H-bond and dispersion interactions and they found that dispersion force can outbalance H-bond with increasing temperatures. Similar vibrational frequencies were observed for the PILs such as triethylammonium methylsulfonate ([Et₃NH][CH₃SO₃]), triethylammonium triflate ([Et₃NH][CF₃SO₃]), trihexylammonium methylsulfonate ([C₆H₁₃]₃NH][CH₃SO₃]), and trihexylammonium triflate ([C₆H₁₃]₃NH)[CF₃SO₃] at low temperatures. However, with increasing temperatures, the bands at 70 and 130 cm⁻¹ decrease, and the new band at about 100 cm⁻¹ increases in intensity, which indicates the change in ionic interactions. DFT calculations suggest that the bands at 70 and 130 cm⁻¹ can be assigned to the bending and stretching modes of the N-H...O₃S H-bonds that dominates at low temperatures, and the band at 100 cm⁻¹ that describes the dispersion interaction between the -SO₃ group and the hexyl groups of the anion. The former dominates at low temperatures, while the latter dominates at high temperatures.

Table 2. Geometries, energies and NCT of the dimers including the different H-bonds from *ab initio* calculations

Dimers ^a	R_{C-H}	$R_{H...X}$	ΔR	$\angle C-H...X$	E_{Elst}^b	E_{Ind}	E_{Disp}	E_{Exch}	NCT ^c
H ₃ C-H...F-H	1.085	2.662	0.000	180	-1.2	-0.2	-1.9	2.1	0.031
H ₃ C-H...F ⁻	1.108	1.855	0.023	180	-40.4	-35.0	-16.2	75.7	0.023
H ₃ C-H...Cl ⁻	1.090	2.665	0.015	180	-12.0	-11.0	-8.5	22.7	0.020
Ion-pair1	1.126	1.899	0.046	159	-434.8	-63.7	-37.8	179.7	0.247
Ion-pair2	1.104	1.991	0.024	148	-400.3	-55.7	-36.0	163.6	0.215
Ion-pair3	1.105	2.012	0.025	150	-405.2	-56.7	-40.6	166.7	0.211
Ion-pair4	1.076	2.693	-0.004	74	-470.6	-63.3	-54.3	199.8	0.241

a. The dimers were optimized by Izgorodina et al.¹¹¹ (Copyright 2012, American Chemical Society) The bond lengths of C-H and H...X and the ΔR values were given in angstroms (Å), and angles of $\angle C-H...X$ were in degrees (°). b. The total energies were dissociated by SAPT, which consists of the Coulomb (E_{Elst}), induction (E_{Ind}), dispersion (E_{Disp}), and Pauli repulsion (E_{Exch}) and these energies were given in kJ/mol.⁸⁹ c. NCT is the net charge transfer.

Three types of π interactions are involved in the imidazolium-based ILs: cation-cation $\pi^+\pi^+$ stacking, cation-anion $\pi^+\pi^-$ and cation-solvent $\pi^+\pi$, which is mainly presented in crystals of the ILs. X-ray studies have revealed the organization of ions connected by π

interactions as exhibited by [PF₆] and [SbF₆] salts in Fig. 5, in which two major arrangements are shown: (1) the arrangement formed by alternating π^+ -anion in columns (A); (2) the arrangement formed

through $\pi^+-\pi^+$ stacking (B) with anions accommodated as chains with anions accommodated as chains.¹¹²

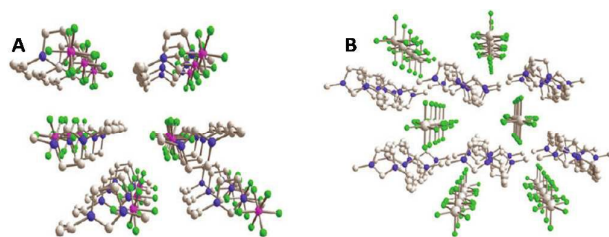


Fig.5 Illustration of the two major arrangements in the crystals of imidazolium ILs.⁴⁰ (Copyright 2007, American Chemical Society)

For the ILs with long alkyl chains cations such as $[C_nC_1im]Br$ ($n = 12-16$), the $\pi-\pi$ stacking from the cation head groups becomes closely relevant with melting points and phase behaviour.¹¹³ Cation-solvent $\pi-\pi$, for example in IL mixtures with benzene has been shown to play a key role in structuring at graphene-IL interfaces.¹¹⁰ MD simulations have also revealed the formation of $\pi-\pi$ interactions in the binary mixture of the ILs $[C_2C_1im][SCN]$ and $[C_2C_1im]Cl$.¹¹⁴ Thus, π -type interactions have been recognised as a key component in the local structures of the imidazolium-based ILs. Hunt et al.⁶⁰ explored the structural and energetic landscape of π interactions of the $[C_1C_1im]Cl$ ion-pair dimer by DFT calculations and found that the π interaction stabilizes the ion-paired dimers by 0–126 kJ/mol energy and the stacking structure exhibits the complex interplay. Fig. 6 shows the Middle and Diagonal conformers with the lowest energy. It can be seen that the Middle conformer shows $\pi^+-\pi^+$ stacking of cations, and the anions locate front and side of cations, while the Diagonal conformer shows the π^+ -anion stacking and the anions locate top of cation and connect with cations by H-bonds. A low barrier (< 6 kJ/mol) for the conversion of Middle to Diagonal conformers indicates that the general conversion from $\pi^+-\pi^+$ stacking (side and front motif) to π^+ -anion stacking (top and front motif) may be a facile process in the liquid phase. The energy differences among the $\pi^+-\pi^+$, anion- π^+ and H-bond is small (< 10 kJ/mol), and their competition creates a very delicate balance of forces within the liquid environment. The dispersion also has a significant impact on for the $\pi^+-\pi^+$ stacking of the rings and the position of Cl^- .

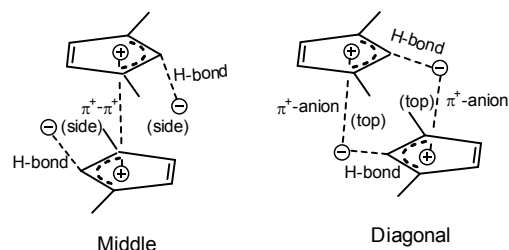


Fig. 6 Structural motifs for the Middle and Diagonal conformers by $\pi-\pi$ interactions.

At this stage, we can conclude that simple generalisation and justification from a conventional H-bond are completely inadequate to understand H-bond in ILs when one attempts to delve into many features of the H-bonds. A model for the H-bond in ILs should be expressed as $(+)X^{\delta+}-H\cdots Y^{\delta-}(-)$, in which X and Y represent the heavy atoms and “+” and “-” stand for the charges of the cation containing X atom and the anion containing Y atom, respectively. Based on this model, we can differentiate the H-bond in ILs from the already well established H-bonds, Zhang et al.¹¹⁵ redefined the H-bond as the Z-bond to describe the features in the geometric, energetic, electronic and assembly aspects. Actually the Z-bond more clearly manifests the cooperation between ion-bond (electrostatic force) and H-bond interactions as shown in Fig. 7 by a cartoon description. Nevertheless, the description of H-bond in gas ion-pairs is not completely appropriate for the H-bonds in liquids and crystals, where the H-bonding network and ionic aggregates are present, but the gas ion-pairs provided direct insight into physical nature of ILs and are the key to understand the bulk behaviour of ILs.

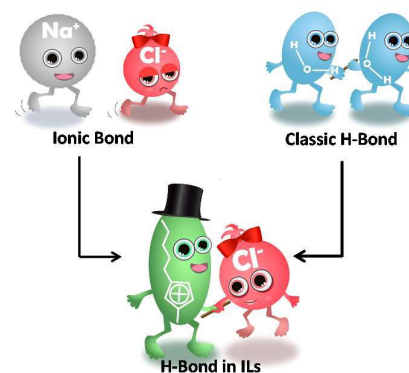


Fig. 7 A description of H-bond in ILs: NaCl is dominated by the electrostatic force between Na^+ and Cl^- , and conventional H-bond is formed between H_2O molecules.

2.3 H-bonding network, ionic aggregate and assembly

Besides asymmetry of cation and anion, which opposes the charge ordering and causes slow-crystallization of the system, the main difference of ILs from the classic molten salts is the presence of the H-bonding network. This makes ions to possess preorganized structures in neat ILs and their mixtures^{38, 116, 117}, resulting in polar and nonpolar nano-domains. Therefore, the ILs cannot be regarded as homogeneous solvents, but can be defined as “supramolecular” fluids.^{118, 119}

The crystal structures of ILs, shown in Fig. 5 can be represented as $[(C)_m(A)_{m-n}]^{n+} [(C)_{m-n}(A)_x]^{n-}$, in which though π -type stacking presents the structural characteristic, the cations and anions are connected by H-bonding network. The H-bonding network has also been identified in liquid state, and a series of supramolecular mono and multiply charged small ionic aggregates with structures of $[(C)_m(A)_{m-n}]^{n+}$ and $[(C)_{m-n}(A)_x]^{n-}$ have been found by ESI-MS

experiments.¹²⁰⁻¹²² Zhang et al.³³ measured IR spectrum of $[\text{C}_2\text{C}_1\text{im}][\text{BF}_4]$ IL and calculated vibrational frequencies of the ion aggregates with different sizes. The good agreement between measured and calculated major bands provided the detailed structural information about the ion organization as shown in Fig. 8. The band at $3000\text{--}3500\text{ cm}^{-1}$ is assigned to the symmetric stretching of cation. Two bands at 1600 and 1500 cm^{-1} can be assigned to the breathing of imidazole rings and the scissoring of the alkyl chains, respectively. The strongest peak at 1136 cm^{-1} is contributed from stretching of B-F bonds of the anion. Though the ionic aggregates present the typical gas structures, they reproduce the vibrational modes reasonably. Thus, these cluster structures can lead to insight into the bulk phase of ILs. The FIR region indicated in the inserted figure exhibits H-bonding interactions. By the comparison between experimental and calculated results, it is found that the stronger band at 122 cm^{-1} is the stretching modes of the $\text{C-H}\cdots\text{F}$ H-bonds, while the band at 86 cm^{-1} is the bending modes of these H-bonds. Furthermore, a cluster of $[\text{C}_2\text{C}_1\text{im}][\text{BF}_4]$ including four ion-pairs is shown in another inserted figure. It can be seen that the ordered ionic arrangements are similar to the crystal structure obtained from X-ray,¹¹² in which the ions are connected by the H-bonds (dashed lines) to form H-bonding network. Neutron diffraction studies of some ILs indicate that charge ordering can endure in the liquid state.^{86, 87} MD simulations for $[\text{C}_2\text{C}_1\text{im}][\text{BF}_4]$ confirm the similar ionic arrangement in bulk liquid phase. The relative strength of H-bonds is corroborated by ESI-MS studies and the relative H-bonding scale can then be estimated by ESI-MS/MS experiments via dissociation of the mixed supramolecular clusters. For the five anions studied, the relative order of intrinsic H-bonding strengths to the fixed $[\text{C}_4\text{C}_1\text{im}]^+$ cation is $[\text{CF}_3\text{CO}_2] > [\text{BF}_4] > [\text{PF}_6] > [\text{InCl}_4] > [\text{BPh}_4]$.

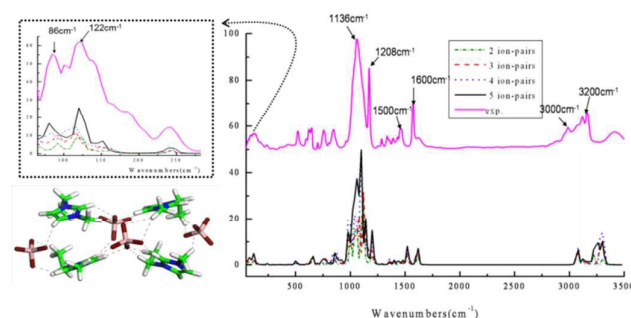


Fig. 8 Comparison of the measured IR spectrum of $[\text{C}_2\text{C}_1\text{im}][\text{BF}_4]$ at room temperature with the vibrational modes of the corresponding ion clusters $([\text{C}_2\text{C}_1\text{im}][\text{BF}_4])_n$ with $n=2, 3, 4, 5$ calculated by DFT at B3LYP/6-31+G** level. The calculated bands were corrected by the factor 0.964-0.967 (Copyright 2012, American Chemical Society).³³

This tendency to form the aggregates held together by H-bonding network is present even in highly diluted solutions and in gas. A series of gaseous supraionic aggregates of the type $[(\text{C}_{n+1}\text{X})_n]^+$ versus their respective anions have been observed by traveling wave ion mobility mass spectrometry. Interestingly, a linear dependence of drift time on the mass of the IL's aggregates indicates an abnormally high mobility for bulkier cations of the ILs.

^{123, 124} Means of atmospheric-pressure chemical ionization mass spectrometry are also used to detect the presence of IL's aggregates by transferring species from the condensed phase to the gas phase, and some neutral clusters of the type $[\text{DAI.X}]_n$ ($n=1, 2,$ and 3) have been observed.¹²⁵ Electric conductivity, NMR, ESI-MS and IR data also support the presence of larger neutral and charged aggregates even when dissolved in solvents with relatively high dielectric constants, such as acetonitrile and dimethyl sulfoxide (DMSO).¹²⁶ The stability and reactivity of the aggregates are dependent on the nature of the anion and imidazolium substituents, and are more abundant in ILs containing strong coordinating anions, in particular those that can form charge transfer complexes.

Fig. 9 shows a MD simulation for the mixtures of $[\text{C}_2\text{C}_1\text{im}][\text{CH}_3\text{CO}_2]$ with water at different molar ratios.¹²⁷ It can be seen that at low water content, water molecules are evenly implanted in the IL (Fig. 9A), and the H-bonding network of the IL is still kept. At an intermediate 50 mol% water content, the H-bonding network of the IL is disrupted and new H-bonding network is formed between ions and water molecules (Fig. 9B), in which each water molecule interacts with two nearby $[\text{CH}_3\text{CO}_2]^-$ anions, and each $[\text{CH}_3\text{CO}_2]^-$ anion in turn interacts with nearby two water molecules. This configuration implies that at the water concentration investigated, the interactions between water molecules and $[\text{CH}_3\text{CO}_2]^-$ anions are optimal. At a high water content of 95 mol%, the IL still behaves as a continuous phase and water molecules are absorbed in the void space formed by the ions (Fig. 9C). This indicates that water not only interacts with the anion and cation, but also alters the cation-anion interaction.

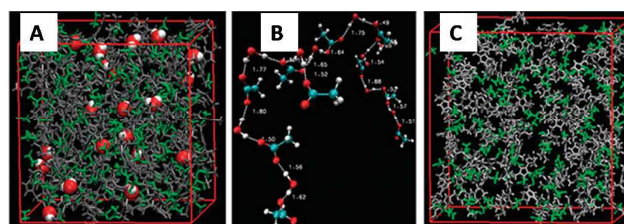


Fig.9 The snapshots from MD simulation at 313 K for the mixtures of $[\text{C}_2\text{C}_1\text{im}][\text{CH}_3\text{CO}_2]$ and water. (A) $X_{\text{water}}=0.11$, the water molecules are shown using the vdw graphical representation. (B) $X_{\text{water}}=0.5$, a H-bonding network consisting of 10 water molecules and 10 $[\text{CH}_3\text{CO}_2]$ anions are shown. For clarity, all other molecules are not shown. (C) $X_{\text{water}}=0.95$, only the $[\text{C}_2\text{C}_1\text{im}][\text{CH}_3\text{CO}_2]$ ions are shown¹²⁷ (Copyright 2015, Royal Society of Chemistry).

Due to the amphiphilic nature of the cations, especially those with the long alkyl chains, the self-assembly has been found in neat ILs and IL solutions.^{118, 128} Zhang et al.¹²⁹ investigated the structure of $[\text{C}_{12}\text{C}_1\text{im}]\text{Br}$ in aqueous solution by MD simulation and found that the initial spherelike structure was evolved into rodlike micelle after 25ns (Fig. 10). It is noted that the whole micelle is separated by the surrounding water to form the different rodlike sub-micelles (see (1), (2) and (3)), in which the heads of cations and anions (red color)

distribute outward and the long chains of cations (green color) distribute inward, and partial Br^- anions diffuse into the water or are solvated by water. In addition to the phase separation between polar and nonpolar groups, the primary characteristics of this structure is that there is also a stronger spatial correlation between the terminal tail-tail groups than between the parts of the chain that are closer to the polar head groups. As such, the tail groups can form prominent aggregation and the aggregates are enhanced by water.¹¹⁸ Furthermore, the main peaks of tail-tail RDFs indicate an interesting turnover.

Such assembly can attribute to a subtle balance of varied interactions. At low water content, the electrostatic force and H-bond between heads of cations and anions make the head groups retain a stable spatial correlation, which causes the continuous enhancement of the tail group aggregation that is dominated by van der Waals interactions between long alkyl chains.^{119, 128} At a range of water contents (~75-80%), the anions are saturated by H-bonds with water so that the electrostatic interaction and H-bonding network between heads of cations and anions are strongly screened by the H-bonds to the anions. Thereafter, electrostatic repulsions of head-head groups are well balanced by the anions and the weak water-head interactions, and the spatial correlation of head groups attenuates, directly resulting in the weakening of tail group aggregation. At higher water content, more and more water molecules destroy the H-bonding network, and the entire system becomes highly diffusive. In this case, a loose micelle structure, with positive charge on the polar "shell" (cation head groups) is formed.

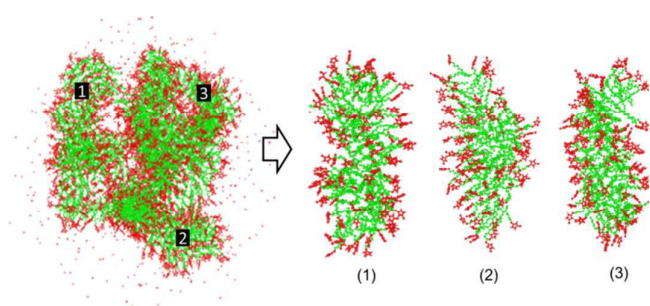


Fig.10 Self-assembly rodlike micelle of $[\text{C}_{12}\text{C}_1\text{im}]\text{Br}$ in aqueous solution and the snapshot presents the rodlike micelle structure from MD simulation at 25ns and water is not shown for clarity. Red and green colors are used to stand for the polar part (imidazolium-ring, the connected C^1 and anion) and nonpolar part (alkyl chain in cation, including C^2 to C^{12}), respectively. (1), (2) and (3) indicate the partial structures of the rodlike micelle.

3. H-bonds in non-imidazolium ILs

3.1 Pyridinium, ammonium and phosphonium ILs

As mentioned in the introduction, the stronger H-bonds in the imidazolium ILs arise from the interaction of anions with the more acidic $\text{C}^2\text{-H}$ of the cation, but other cations such as pyridinium, pyrrolidinium and quaternary ammonium and phosphonium only

have the weak H-bonding interactions with anions due to the fact that they do not carry a specific acidic proton. However, α -hydrogen is acidic and able to facilitate the formation of H-bonds.

In the *N*-ethylpyridinium tetrafluoroborate ($[\text{C}_2\text{py}][\text{BF}_4]$) ion-pair optimized by *ab initio* calculation, it is found that the $[\text{BF}_4]^-$ prefers to locate above the pyridinium ring and has close contact with the nitrogen atom.⁸⁴ The $\text{N}\cdots\text{B}$ distance is 3.21-3.62 Å. Notably in some ion-pairs, the $[\text{BF}_4]^-$ is close to the α -hydrogen and the $\text{C}^2\text{-H}\cdots\text{B}$ distance is 2.45-2.82 Å, which indicates H-bonding interaction with C-H. It is also found that the $[\text{BF}_4]^-$ is close to the β -hydrogens at $\text{C}^3\text{-H}$ and $\text{C}^4\text{-H}$, but the $\text{C}^{3/4}\text{-H}\cdots\text{B}$ distances (2.64-2.84 Å) are longer than α -hydrogen, suggesting a weaker H-bonding interaction. The positive charge on pyridinium is distributed mainly on the nitrogen atom and carbon atoms of $\text{C}^2\text{-H}$, $\text{C}^3\text{-H}$ and $\text{C}^4\text{-H}$, which explains the reason for the formation of the conformations. The calculated interaction energies, ΔE of the most stable ion-pairs are 346.27 and 332.05 kJ/mol, suggesting that the $[\text{BF}_4]^-$ prefers to have close contact with the nitrogen atom and the α -hydrogen atom of $\text{C}^2\text{-H}$. For the quaternary ammonium ion-pairs, such as *N*-ethyl-*N,N,N*-trimethylammonium tetrafluoroborate ($[(\text{C}_2\text{H}_5)(\text{CH}_3)_3\text{N}][\text{BF}_4]$), the $[\text{BF}_4]^-$ locates between two alkyl chains and the central $\text{N}\cdots\text{B}$ distance is 3.92 Å for the lowest energy conformation. Three F atoms are close to the α -hydrogens of alkyl chains and the $\text{C-H}\cdots\text{F}$ distance is 3.19-3.24 Å, indicating very weak H-bonding interactions. The calculated ΔE values for the most stable ion-pairs are 353.79 and 350.87 kJ/mol. The phosphonium-based ion-pairs show very similar structures and energies with quaternary ammonium ion-pairs, and the α -hydrogen atoms are acidic and can form H-bonds with anion, which is very useful for facilitating chemical reactions.¹³⁰⁻¹³²

In the mixtures of the ILs with some cosolvents, such as water and DMSO etc., the H-bond is critical to stabilize the systems. Wang et al.¹³³ characterized the H-bonds between the *N*-butylpyridinium tetrafluoroborate ($[\text{C}_4\text{py}][\text{BF}_4]$) and water or DMSO by using attenuated total reflection Fourier transform infrared (ATR-FTIR) spectroscopy and DFT calculations. It is found that H-bond is the main interaction between ions and molecules and the strength of H-bond between cation and anion is comparable with that between the cation and water. Water molecules preferentially interact with the $[\text{BF}_4]^-$ anion by forming anion $\cdots\text{HOH}\cdots$ anion H-bonding model. Both water and DMSO can interact with the pyridinium cation, and the favorable sites are the α -hydrogen atoms of C-H. The interactive pattern is related with charge distribution. The alkyl groups linked to the H-bond acceptor are electron-donating, while those connected to the H-bond donor are electron-withdrawing, both of them make positive contributions to the stability of the H-bond. Zhang et al.¹³⁴ investigated the interaction between *N*-butylpyridinium cyano ($[\text{C}_4\text{py}][\text{SCN}]$) IL and DMSO by ATR-FTIR, ^1H NMR and DFT calculation. It is found that H-bonds are universally involved and play an important role for the miscibility of DMSO with $[\text{C}_4\text{py}][\text{SCN}]$ IL and the stability of this system. With the addition of DMSO, the H-bonding interactions involving the alkyl C-Hs and $\text{C}\equiv\text{N}$

are strengthened, while the H-bonds involving C–Hs of the pyridinium ring are weakened. Lauw et al.¹³⁵ investigated the effect of water on the surface structure of 1-butyl-1-methylpyrrolidinium bis(trifluoromethylsulfonyl)imide ($[\text{C}_4\text{C}_1\text{pyr}][\text{NTf}_2]$) IL by X-ray reflectometry and MD simulations, and they found that the first layer of the gas-liquid phase boundary was occupied mainly by a mixture of cations and water.

3.2 H-bonds in PILs

3.2.1 H-bonds in ion-pairs

PILs show the strong H-bonding interaction, by which the proton transfer occurs between the acid and base.⁵¹ From the data listed in Table 1, such H-bonds have been compared with H-bonds in common ILs. It is clear that the PILs, such as $[\text{EtNH}_3][\text{NO}_3]$, $[\text{PropNH}_3][\text{NO}_3]$ and $[\text{Me}_3\text{NH}]\text{Cl}$ show much larger $E_{n\rightarrow\sigma^*}^{(2)}$ values than the common ILs. For the alkylammonium-based PILs, the $\text{N}\cdots\text{Y}$ H-bonds are stronger when the acceptor Y is O atom than that when the acceptor is the N or S atom.⁵⁰ Bodo et al.⁵⁴ found from DFT calculations and Raman spectroscopy that the H-bonds determine directionality of ionic interaction and are more important than the electrostatic force. Hunger et al.⁵² studied the molecular rotation of the $[\text{EtNH}_3][\text{NO}_3]$ by probing the ammonium N–H vibrations with dielectric relaxation and femtosecond infrared spectroscopy, and they found that the rotation of cation take place via large angular jumps, which indicates that the strong intermolecular interaction is highly directional in this class of ILs. Neutron diffraction provides the structural details of H-bonds in the alkylammonium PILs,¹³⁶ and it is found that both length and angle of the H-bonds vary with the anions and cations. For example the lengths of H-bonds in $[\text{EtNH}_3][\text{SCN}]$ (1.71 Å) and $[\text{EtNH}_3][\text{HSO}_4]$ (1.62 Å) are much shorter than that in other PILs. The probability distribution of the angle for the short H-bonds shows a close linear $\text{N}\cdots\text{H}\cdots\text{Y}$ arrangement (the maxima at 180°). Conversely, the H-bonds with long bond length is bent (the maxima at 110°). The coexistence of two H-bonds shows the characteristics of the PILs and the difference from the common ILs.

In mixtures of PILs with molecular solvents, the contact ion-pair (CIP) is found to be the main ion speciation at low concentration. In the CIPs, long-range electrostatic forces as well as short-range directed H-bonds hold the cation and anion together, which is different from the hydrophobic imidazolium ILs, where CIPs are formed at high concentration.^{58, 137} With the addition of a molecular solvent, the CIPs can be changed into solvent-separated ion-pairs (SIPs) and the H-bonds are disrupted. It is found from DFT calculation that four and more water molecules are needed for the transition of CIPs to SIPs in $[\text{Et}_3\text{NH}][\text{CH}_3\text{SO}_3]$ -water mixture as shown in Fig. 11.^{58, 138}

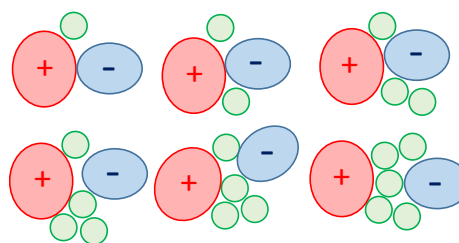


Fig. 11 Schematic illustration for the transition of CIP into SIP by the addition of molecular solvents in the PILs.

3.2.2 H-bonding network and ion aggregate

The strong H-bonds in the PILs result in the formation of 3D H-bonding network as in water. Taking $[\text{EtNH}_3][\text{NO}_3]$ as an example, it is interesting to see whether the PIL also displays some of the unique structures like water. Evans et al.¹³⁹⁻¹⁴¹ reported that $[\text{EtNH}_3][\text{NO}_3]$ possesses some similarities with water. In particular, the phase transfer of rare gases and hydrocarbons from cyclohexane to this PIL is accompanied by negative enthalpy and entropy changes. Obviously the $[\text{EtNH}_3][\text{NO}_3]$ shares the ability with water to form a 3D H-bonding network. However, the strength of the H-bonding network in $[\text{EtNH}_3][\text{NO}_3]$ is only half that in water. Per solvent ion can form only three H-bonds in $[\text{EtNH}_3][\text{NO}_3]$, and in addition to the Coulomb force, the tetrahedral structure of the cation, and in addition to the Coulomb forces the planar structure of the anion must impose a very different type of solvent ordering from water. DFT calculations for the $[\text{EtNH}_3][\text{NO}_3]$ suggest that the tetrahedral structure of H-bonding network only occurs in water, whereas it is missing in the $[\text{EtNH}_3][\text{NO}_3]$.⁵³

Large ion aggregates through H-bonding network have been observed in PILs. Fig. 12 shows the ESI-MS results for $[\text{EtNH}_3][\text{NO}_3]$ PIL, and the C_6A_7^+ ion aggregate is the most prominent in the liquid.¹⁴² This aggregate is visibly larger than that in the imidazolium-based ILs, where the C_2A^+ is the major aggregate. These aggregates with different sizes are also investigated by DFT calculations as the structures shown in Fig. 12. With increasing sizes, the aggregates change from ordered to disordered structures. The two and four ion-paired aggregates show cubic-like arrangement but the six and eight ion-paired aggregates already show a high degree of structural disorder.⁵⁴ The aggregates may be stabilized by two opposite forces: one is H-bond that promotes the ordered structure, and another is the apolar alkyl chains that prevent the formation of the ordered structure. It is found that some of the nitrate anions tend to form only two H-bonds, and leave one of their acceptor sites almost free in the clusters. This, together with the finite size effect, leads to a dispersion of the N–H stretching vibrational frequencies in the calculated clusters between 2800 and 3400 cm^{-1} . This dispersion is also present in the experimental spectra, thereby pointing to a sort of unsaturation effect of the H-bonding network in the “real” liquid.

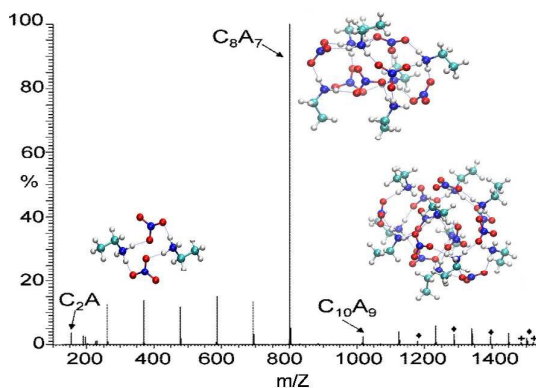


Fig. 12 ESI-MS positive ion mode of anhydrous $[\text{EtNH}_3][\text{NO}_3]$ and different sizes of ion aggregates obtained by DFT calculations.

4. Experimental evidences for H-bonds by low-frequency spectroscopy

Although H-bonds have been well characterized by calculations, the experimental evidences are still challenging. Fumino and Ludwig et al.^{44, 66} have found that low frequency vibrational spectroscopy within the range of 30–300 cm^{-1} , equivalent to 0.3–9 THz or 1–36 meV, for example far infrared (FIR) and terahertz (THz) spectroscopy is suitable for the characterization of the H-bonds in ILs. Combining with DFT calculations, the obtained frequencies were assigned rationally. The characteristics of H-bonds was mainly focused on the stretching (ν_a) and bending (ν_b) vibrational modes as shown in Fig. 13A. In fact, the vibrations are very sensitive to the force constant κ and the reduced mass μ . In order to eliminate shift of frequency caused from the μ , the ions are usually required to have the similar μ value. 13B shows the FIR spectra of the ILs with $[\text{C}_2\text{C}_1\text{im}]^+$ cation and the anions $[\text{N}(\text{CN})_2]^-$ (1), $[\text{SCN}]^-$ (2), $[\text{NO}_3]^-$ (3) and $[\text{CH}_3\text{COO}]^-$ (4) that have similar μ value.¹⁴³ It can be seen that the FIR bands shift to the higher frequency in the order of 1–4, which indicates that the H-bonding interactions between the cations and anions are enhanced. The largest shift of 22 cm^{-1} found for $[\text{C}_2\text{C}_1\text{im}][\text{CH}_3\text{COO}]^-$ (4) indicates the strongest H-bonding strength. This result is supported by DFT calculation and the H-bonding energy (35 kJ/mol) for the IL 4 is higher than that for 1–3 ILs.⁴²

Fig. 13C shows the FIR spectra of the ILs with the same $[\text{NTf}_2]^-$ anion and different cations, such as 1, 2, 3-trimethyl-imidazolium $[\text{C}_1\text{C}_1\text{C}_1\text{im}]^+$ (1), 1, 3-dimethyl-imidazolium $[\text{C}_1\text{C}_1\text{im}]^+$ (2), 1, 2-

dimethylimidazolium $[\text{C}_1\text{C}_1'\text{im}]^+$ (3) and 1-methyl-imidazolium $[\text{C}_1\text{im}]^+$ (4).¹⁴⁴ The cation $[\text{C}_1\text{C}_1\text{C}_1\text{im}]^+$ is formed by methylation of the $[\text{C}_1\text{C}_1\text{im}]^+$ at C^2 position, such a selection makes the vibrational bands associated with the H-bond to disappear consequently. The cation $[\text{C}_1\text{C}_1'\text{im}]^+$ is designed by substitution of a methyl of $[\text{C}_1\text{C}_1\text{im}]^+$ connected with nitrogen atom for a proton. The cation is chosen to consider the $\text{N-H}\cdots\text{anion}$ H-bond. The $[\text{C}_1\text{im}]^+$ cation has only a methyl connected nitrogen atom. It can be seen that the vibrational bands with the maximum intensity are below 150 cm^{-1} ,¹⁴⁵ but the frequencies shift to higher wavenumbers in the order from 1 to 4, which is consistent with the H-bonding strength. In 1, the H-bonding interaction is weakened by methylation at C^2 position, but in 2 and 3, there are H-bonds either via the $\text{C}^2\text{-H}$ or N-H , whereas in 4 all of the H-bonds are possible, which suggests that the potential H-bond capabilities are increased on the assumption that other interactions are not changed.⁴¹ Fig. 13D shows the FIR spectra of the common ILs $[\text{C}_4\text{C}_1\text{C}_1\text{im}][\text{BF}_4]^-$ (1), $[\text{C}_4\text{C}_1\text{im}][\text{BF}_4]^-$ (2) and $[\text{C}_4\text{C}_1\text{im}][\text{NO}_3]^-$ (3) and the PIL propylammonium ($[\text{propNH}_3][\text{NO}_3]^-$) (4).¹⁰² It can be seen that the vibrational bands of 1, 2 and 3 have the maximum intensity below 150 cm^{-1} , but the frequencies are shifted to higher wavenumbers. For 1 and 2, the anions are same and the interactions are enhanced by methylation at the C^2 position from the $[\text{C}_4\text{C}_1\text{mim}]^+$ to $[\text{C}_4\text{C}_1\text{im}]^+$. Then the weak interacting anion $[\text{BF}_4]^-$ is replaced by the strongly interacting anion $[\text{NO}_3]^-$ from 2 to 3. For the PIL $[\text{PropNH}_3][\text{NO}_3]^-$, the maximum intensity of the FIR modes were observed below 250 cm^{-1} . The shift of 100 cm^{-1} to higher frequency indicates that the H-bonding strength is enhanced distinctly. DFT calculations suggest that the frequencies at about 224 cm^{-1} and 159 cm^{-1} can be assigned to the ν_a modes (asymmetry ν_{as} and symmetry ν_s) of the H-bonds $\text{N-H}\cdots\text{O}$ and the vibrational bands at 78 cm^{-1} can be assigned to ν_b modes of the H-bonds.¹⁰²

Such conclusion that the stronger H-bonds shift the frequencies to higher wavenumbers can be used to study the interaction strength as a function of temperature and phase transition. Another possibility is to analyse the change of interaction energies in ILs solution. In diluted ILs, it is possible to study whether ion-pair or cluster formation leads to stronger anion–cation interaction compared to that in the neat liquids. In principle, FIR spectroscopy in combination with DFT calculations and/or MD simulations is very suitable for studying ILs and their mixtures. The shift of frequencies can also be correlated with the properties of ILs, for example a linear relationship was found between enthalpy of vaporization and the shift of frequencies in imidazolium-based ILs,¹⁴⁶ which manifests the role of H-bonds in the properties as stated in the following section.

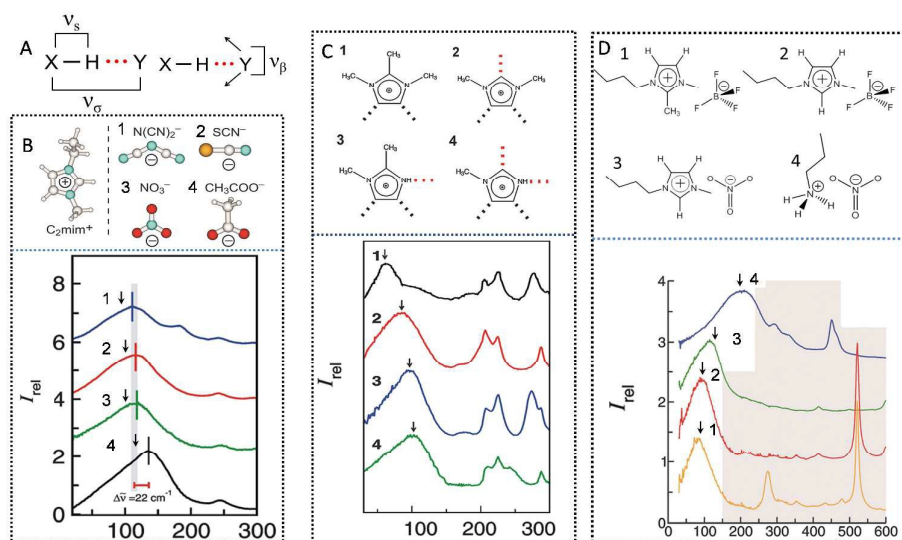


Fig. 13 Far infrared spectra (FIR) measured by Bruker VERTEX 70 FTIR spectrometer for different ILs. (A) Schematic stretching (ν_s) and bending (ν_β) vibrational modes of X-H...Y H-bond in IL. (B) FIR spectra of $[\text{C}_2\text{C}_1\text{im}][\text{N}(\text{CN})_2]$, $[\text{C}_2\text{C}_1\text{im}][\text{SCN}]$, $[\text{C}_2\text{C}_1\text{im}][\text{NO}_3]$ and $[\text{C}_2\text{C}_1\text{im}][\text{CH}_3\text{COO}]$ (Copyright 2012, American Chemical Society).¹⁴³ (C) FIR spectra of $[\text{C}_1\text{C}_1'\text{im}][\text{NTf}_2]$ (1), $[\text{C}_1\text{C}_1'\text{im}][\text{NTf}_2]$ (2), $[\text{C}_1\text{C}_1'\text{im}][\text{NTf}_2]$ (3), $[\text{C}_1\text{im}][\text{NTf}_2]$ (4) at 323 K for 2–4 and 383 K for 1 (Copyright 2010 WILEY-VCH Verlag GmbH & Co. KGaA, Weinheim).¹⁴⁴ (D) FIR spectra of $[\text{C}_4\text{C}_1\text{C}_1'\text{im}][\text{BF}_4]$, $[\text{C}_4\text{C}_1\text{im}][\text{BF}_4]$, $[\text{C}_4\text{C}_1\text{im}][\text{NO}_3]$ and $[\text{PrAm}][\text{NO}_3]$ at 353 K (Copyright 2009, Royal Society of Chemistry).¹⁰²

5. The correlation with properties

Some properties of ILs are closely relevant with their H-bonds. It is estimated that the H-bond contribution is 30-50 kJ/mol and 10%-16% of the overall interaction energy. Thus, regulation of the ILs properties by changing the H-bonding interaction is fundamentally important for the design of new ILs. It is now shown that H-bond is of significant importance, and in some case, even small local interactions can lead to characteristically different physicochemical properties.^{43,44}

The change in ILs of properties resulted from the H-bonds can be checked by methylation of $\text{C}^2\text{-H}$ of the imidazolium ring to eliminate the effect of H-bonds, and such strategy has been discussed above in Fig. 13. Nevertheless, Kirchner and Hunt et al.^{98,147} found by using X-ray photoelectron spectroscopy (XPS), NMR and DFT calculations that H-bond and charge transfer is independent each other for the imidazolium ILs, which suggests that other interactions, especially electrostatic interaction are not changed substantially. Fig. 14 shows the changes of the melting point (T_m), viscosity (η) and enthalpy of vaporization ($\Delta_{\text{vap}}H$) along the anions in the protonated $[\text{C}_2\text{C}_1\text{im}]\text{X}$ ILs with $\text{C}^2\text{-methylated}$ $[\text{C}_2\text{C}_1\text{C}_1'\text{im}]\text{X}$ ILs (X is a serial of anions).¹⁴⁸ It can be seen that the T_m and η values are increased from $[\text{C}_2\text{C}_1\text{im}]\text{X}$ to $[\text{C}_2\text{C}_1\text{C}_1'\text{im}]\text{X}$. It is expected that the addition of a methyl group increases the molecular volume and that leads to higher T_m and η .¹⁴⁹ However, these effects do account only partially for the significant changes of the properties. Bonhôte et al.⁸ found that methylation at the $\text{C}^2\text{-H}$ position in $[\text{C}_2\text{C}_1\text{im}][\text{NTf}_2]$ increases the η values substantially from 34 mPa·s to 88 mPa·s, whereas it is only less affected ($\eta = 37$ mPa·s) for methylation at the $\text{C}^5\text{-H}$ position. The same behaviour is also found for the T_m . This

result may be explained by considering the fact that the C^2 proton of $[\text{C}_2\text{C}_1\text{im}]^+$ cation can engage in stronger H-bonding with the anions than $[\text{C}_2\text{C}_1\text{C}_1'\text{im}]^+$ cation. However, MacFarlane et al.^{111,150} believed that the increase in T_m and η values was related with the potential energy surface profiles when the anion moves around the imidazolium ring. The potential energy surfaces reveal that the anion was restricted the conformations of above/below the imidazolium ring with for the $\text{C}^2\text{-methylated}$ $[\text{C}_2\text{C}_1\text{C}_1'\text{im}]\text{X}$ ion-pair, and the potential barrier that separates the two conformations exceed 40 kJ/mol, whereas for the protonated $[\text{C}_2\text{C}_1\text{im}]\text{X}$ ion-pair, the anion can freely move around, while staying strongly bound with the cation. Consequently, the methylated imidazolium ILs exhibit much higher T_m and η values than the non-methylated imidazolium ones. Maginn et al.¹⁵¹ performed MD simulation for $[\text{C}_2\text{C}_1\text{im}][\text{PF}_6]$ and $[\text{C}_2\text{C}_1\text{C}_1'\text{im}][\text{PF}_6]$ ILs and found that the entropy is likely an important factor in determining the T_m and η values of the ILs. Interestingly, although less H-bonds were formed in $\text{C}^2\text{-methylated}$ $[\text{C}_2\text{C}_1\text{C}_1'\text{im}][\text{PF}_6]$ ILs, more stable ion cages were observed for this IL.

The effect of H-bond is also clear for the measured $\Delta_{\text{vap}}H$ as shown in Fig. 14A, in which the $\Delta_{\text{vap}}H$ values of $[\text{C}_3\text{C}_1\text{C}_1'\text{im}]\text{X}$ (X=anion) increase though the $[\text{C}_3\text{C}_1\text{C}_1'\text{im}]^+$ and $[\text{C}_4\text{C}_1\text{im}]^+$ cations have nearly identical molecular volume. Furthermore, Ludwig et al.¹⁴⁶ measured FIR spectra of 11 imidazolium-based ILs (Fig. 14B) with the $[\text{C}_2\text{C}_1\text{im}]^+$ cation and a series of anions and they obtained a linear relationship between $\Delta_{\text{vap}}H$ values and the vibrational frequencies. From fitting of the experimental data, the following linear equation was obtained:

$$\Delta_{\text{vap}}H = 75.1 \text{ kJ/mol} + 0.75 \text{ kJ/mol} \cdot \text{cm}^{-1} \times \nu \quad (2)$$

where ν is the wavenumber. The linear relationship reflects the effect of the weak interactions on the physicochemical property. Such a relationship opens a new path for predicting properties by using spectroscopic measurements.

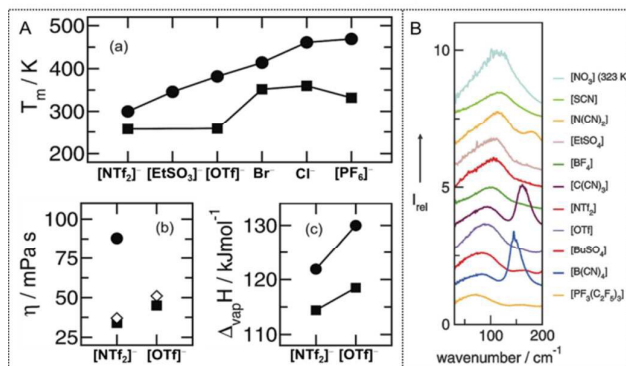


Fig. 14 A. Anion dependence of T_m , η and $\Delta_{vap}H$ values for the imidazolium-based ILs with protonated and C² methylated cations. ¹⁴⁸ (a) T_m of [C₂C₁im]⁺ (squares) and [C₂C₁C₁im]⁺ (circles) containing a series of anions, (b) η of [C₂C₁im]⁺ (squares) and [C₂C₁C₁im]⁺ (circles) with anions [NTf₂]⁻ and [OTf]⁻ anions, and η for methylated ILs at the C⁵ position (diamonds), (c) $\Delta_{vap}H$ of [C₄C₁im]⁺ (squares) and [C₃C₁C₁im]⁺ (circles) with anions [NTf₂]⁻ and [OTf]⁻ (Copyright 2009, WILEY-VCH Verlag GmbH & Co. KGaA, Weinheim). B. The measured FIR spectra for 11 imidazolium-based ILs with a series of anions (Copyright 2010, WILEY-VCH Verlag GmbH & Co. KGaA, Weinheim).¹⁴⁶

Some physical properties are relevant with volume, symmetry and packing of ions. Borodin et al.¹⁵² reported a relationship between η and $\Delta_{vap}H$ as shown in Equ. 3, which suggests that for the same class of liquids $\Delta_{vap}H$ is strongly correlated with the activation energy for viscosity, and the barrier height that molecules should overcome for diffusion/rotation.

$$\eta V_m \sim RT \exp(\alpha H_{vap} / RT) \quad (3)$$

The $\Delta_{vap}H$ values of [C_nC₁im][NTf₂] (n=2–8) ILs were correlated with surface tension (σ) and molar volume (V_m) of the ILs.^{153, 154} An empirical relation for the molar enthalpy of vaporization is given by Equ. 4, where N_A is the Avogadro constant, and A and B are constants.

$$\Delta_{vap}^g H_m(298) = A(\sigma V_m^{2/3} N_A^{1/3}) + B \quad (4)$$

The $\Delta_{vap}H$ values of the pyridinium-based ILs [C_npy][NTf₂] (n=2, 3, 4) were measured in the temperature range of (493–516 K) by using the Knudsen Effusion combined with a quartz crystal microbalance.¹⁵⁵ The volatility is five times lower than that of the imidazolium ILs with the same anion and alkyl chain, which is driven by their higher enthalpy of vaporization e.g. the vapor pressure is 0.04 Pa for the [C_npy][NTf₂] ILs and is 0.2 Pa for the [C_nC₁im][NTf₂] ILs at T = 490 K. This observation is in agreement with a higher charge localization of the pyridinium cation as reflected in their higher enthalpies of

vaporization. The interactions between the ions involves not only Coulomb interaction, but also van der Waals and H-bonding interactions, leading to a complex structural/nanostructural organization, which contributes to the higher thermal stability of ILs. In addition, the *N*-alkylpyridinium based ILs present an aromatic character with significant contribution to the π - π interactions and charge delocalization of the aromatic moiety. Their aromatic character contributes also to the high thermal stability of both cations.

H-bond has also important effect on the properties of PILs, and the glass transition temperature (T_g), T_m , boiling point (T_b), η and ionicity are relevant with H-bond. The T_g value is an indicative of the cohesive energy, which is decreased by repulsive Pauli force and increased by the attractive Coulomb, H-bond and van der Waals interactions. Hence, T_g values can be controlled through modifying the interactions between the cation and anion.¹⁵⁶ The T_m values have a broad range from below room temperature to above 100°C. Many factors can influence the T_m values and the key factor involves sufficient steric hindrance to disrupt the packing efficiency and minimize the H-bonding interaction. The PILs containing [NTf₂]⁻ have lower T_m values, which has been ascribed to the relatively large radius of the anion to weaken the electrostatic interaction with the cation. However, the low T_m values for the salts with the [BF₄]⁻ anion are not consistent with this trend.¹⁵⁷ It is recognized that the H-bond is likely to play more important role than the radius of ions. The η values are more dependent on H-bonds and van der Waals interactions, and stronger interactions lead to higher η values. It can be seen from the plot of T_g against η that the structures of anions have a far greater effect on the viscosity than that of the cations, which can be explained by the fact that the anions are capable of forming the stronger H-bonding network with the cation leading to the higher viscosity of the ILs. For the cations, such as alkylammonium cations, the η values increase with increasing alkyl chain length and significantly increase with hydroxyl or methyl substitution onto the alkyl chain. Tributylammonium nitrate has a particularly high viscosity due to an increase in both H-bonds and van der Waals interactions from the three chains. The vaporization of [EtNH₃][NO₃] was investigated by experimental thermogravimetric analysis with time of flight mass spectrometry (TGA-ToF-MS).¹⁵⁸ It is found that [EtNH₃][NO₃] has a low vapour pressures and a high $\Delta_{vap}H$ of about 105.3 kJ/mol. Starting from 419 K, the decomposition to nitric acid and ethylamine becomes more thermodynamically favourable than proton transfer.

It is known that in PILs, proton transfer is not necessarily complete, which may cause the coexistence of ions and neutral molecules in the PILs. Therefore, ionicity is especially important for PILs. Actually, Walden plot is based on Walden rule: $\Lambda \eta = \text{constant}$,¹⁵⁶ where Λ stands for equivalent conductivity (the conductivity per mole of charge) and η presents the viscosity (η^{-1} is also called fluidity). It is clear that Walden plot can be used for organizing the relations between equivalent conductivity and fluidity. Usually, Walden plot is constructed by plotting $\log(\Lambda)$ against $\log(\eta^{-1})$, and the data for a dilute aqueous KCl solution are also included to fix the position of

the “ideal” Walden line. Any departure from the ideal Walden line is a strong indicative of the existence of a fraction of ion pairs and/or ionic aggregates. By using this method, it is found that the PILs generally show poor ionicity.¹⁵⁷ MacFarlane et al.¹⁵⁹ measured the Walden plot of a series of ammonium acetate ILs and found that the primary amines exhibit a “close-to-ideal” behaviour and produce highly ionized ILs, whereas tertiary amines sit far below the ideal line ($DW > 1$) and tend to form mixtures with a low degree of proton transfer. Nevertheless, Walden plot is unable to distinguish between low ionicity in ILs at a low degree of proton transfer.¹⁵⁹ Angell et al.^{157, 160} also used aqueous pK_a values as the basis to estimate the degree of proton transfer in PILs and they observed $\Delta pK_a > 10$ to be required for the full proton transfer to occur in the PILs and some PILs with $\Delta pK_a > 8$ show nearly ideal Walden behaviour. This result is somewhat surprising given that simple equilibrium calculations indicate that $\Delta pK_a(aq) = 4$ is sufficient to produce 99% proton transfer in aqueous solution, indicating that $\Delta pK_a(aq)$ is a relatively poor estimation for the effective ΔpK_a in the IL environment. This suggests that solvation environment of ILs may have a strong effect on the proton transfer by H-bonds.

6. The role of H-bonds in enhancing the reactions

Besides the correlation with the physicochemical properties, the H-bond plays a crucial role in many applications of ILs^{39, 161}. Importantly, many reactions are related with the H-bonding, and which demonstrated to reduce reaction energy barrier and to stabilize key TS, even the H-bond is used to control supramolecular aggregation of biological macro-molecules,¹⁶² and microscopic ordering into domains⁶¹.

6.1 CO₂ absorption and conversion

As the main greenhouse gas contributing to the global warming, CO₂ has attracted increasing attentions. Recently, ILs have brought the potential breakthrough in the field of the absorption and conversion of CO₂. It is reported¹⁶³ that CO₂ exhibits good solubility in the IL 1-hexyl-3-methylimidazolium hexafluorophosphate ([C₆C₁im][PF₆]) and 0.0881% increase in mass of the IL manifests the absorption. Furthermore, some amino-functionalized ILs can chemically absorb CO₂ and the molar uptake approaches 0.5 stoichiometry during the 3h exposure, showing more advantage than the physical absorption.¹⁶⁴ The amino functionalized ILs, such as ILs with sulfone and amino acid anions are reported to reach 0.5 absorptive stoichiometry.^{165, 166} Brennecke et al.¹¹ reported that trihexyl (tetradecyl) phosphoniumproline ([P₆₆₆₁₄][Pro]) and methionine ([P₆₆₆₁₄][Met]) ILs could absorb CO₂ in 1:1 stoichiometry. Studies on mechanism have found that the H-bond plays important roles in the chemical absorption. Fig. 15 shows MO energy-level diagram of CO₂ and the functional 3-propylaminoimidazolium-1-butylimidazolium tetrafluoroborate ([pabim][BF₄]) or tetramethylguanidinium lactate ([tmg]L) ILs with -NH₂ groups. The energy barriers are 9.26 and 12.82 eV between the LUMO of CO₂ and HOMO of [pabim]⁺ and of [tmg]⁺ cations, however, the energy barriers are 6.07 and 9.53 eV between the LUMO of CO₂

and the HOMO of [pabim][BF₄] or [tmg]L ion-pairs in which the anion and cation are connected by H-bond. The reduced energy barriers indicate the easier reaction between CO₂ and the -NH₂ group when H-bonds is present in the ion-pairs.³⁹

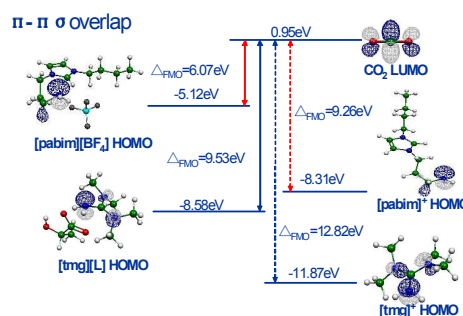


Fig. 15 MO energy-level diagram of CO₂ and the functional ILs [pabim][BF₄] and [tmg]L with -NH₂ groups.

CO₂ conversion into fuel additives is in another efficient category. In the conversion reactions, the hydrogen bond donor (HBD)/IL catalyst has attracted more attentions, because this kind of system exhibits better tolerance to water compared with Lewis acid/IL systems. An example of the reaction is IL catalytic CO₂ conversion to cyclic ethylene and propylene carbonates. DFT calculations illustrated that the presence of HBDs, such as the compounds containing hydroxyl groups, can play a positive role on lowering the barrier and accelerating the ring opening of epoxide (Fig. 16A). Zhang et al.^{167, 168} reported that the presence of water could remarkably improve the activity of ILs, by which the turnover frequency of the reaction is about 4–5 times higher than that in the absence of water. The reaction route is very different from that in Lewis acid/IL systems (Fig. 16B). Zhang et al.¹⁶⁷ screened more effective HBD for the fixation of CO₂ with propylene oxide (PO) in the presence of HBD and 1 mol% quaternary ammonium IL ([Bu₄N]Br) and they found that in the presence of stronger HBD, such as phenol and acetic acid, PO conversion was remarkably enhanced to 95%. This result demonstrates that the enhanced activity is in well accordance with the binding energy and the H-bond distance.

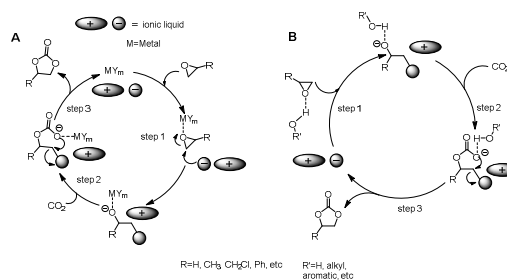
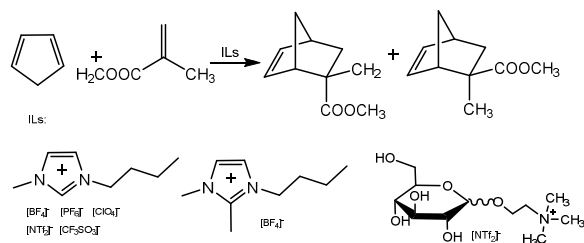


Fig. 16 The proposed mechanisms for Lewis acid/IL system. (A) HBD/IL system, (B) IL catalyzed synthesis of cyclic carbonates.

6.2 Diels-Alder addition reaction

Many methods have been developed to enhance Diels-Alder reaction, but so far the most effective catalyst is generally considered to be the Lewis acids. Recently, the increasing interests are focused on the use of ILs as catalyst.¹⁶⁹ Kinetic and stereochemical investigations have been performed on model Diels-Alder reactions to evaluate the ability of ILs to affect *endo/exo* selectivity and reaction rate.¹⁷⁰ The influence of ILs on Diels-Alder addition of cyclopentadiene with methylacrylate as model reaction has been investigated extensively. The employed ILs were based on the $[C_4C_1im]^+$ and $[C_4C_1C_1im]^+$ cations as shown in Scheme 1.¹⁷¹



Scheme 1 Diels-Alder reaction of cyclopentadiene with methyl methacrylate and the ILs used in the reaction.

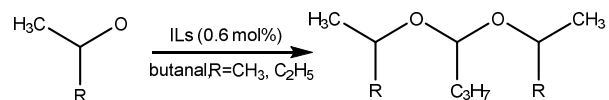
Associated enhancement observed in the Diels-Alder reaction attributes to the ability of the IL to form H-bond with the dienophile (methyl acrylate). The process is considered by two competing equilibria. One is formation of H-bonds of cation ($[C_4C_1im]^+$) with anion (equilibrium 1, equilibrium constant K_1), and another is the cation form H-bonds with the methyl acrylate (equilibrium 2, equilibrium constant K_2). It has been proposed that the concentration of the H-bonding cation-methyl acrylate adduct is inversely proportional to the equilibrium constant for the formation of the cation-anion H-bonding adduct (K_1). From analysis of the structure, it is found that though the equilibrium 1 represents the dissociation of an ion-pair, the ILs should be described as a 3D H-bonding network of anions and cations, in which each ion is surrounded by several counterions. The interaction of a cation with reagents and/or the TS reduces of the interactions of this cation with the surrounding anions. The competition results in the reorganization and reorientation of the solvent around solute, which disfavors the formation of a cavity and reduces the possibility for the cation (or anion) to solvate the reagent and/or the TS.¹⁷² However, the situation is much more complicated than that represented by equilibrium 1 and 2, in which kinetic plays a role during the solvent reorganization and reorientation. The concept of ion-pair association and dissociation, widely used for solutions of ionic compounds in molecular solvents, probably can't be transferred as it stands to ILs.¹⁷³

H-bonding groups, such as hydroxyl, carboxyl, nitrile and benzyl groups on the cation increase the *endo* selectivity.¹⁷⁴ However, the reduced ability of H-bond in 1-alkyl-2,3-dimethylimidazolium ILs (bearing a methyl group at C_2 position) gives a selectivity of 4.4 for the *endo:exo* ratio in $[C_4C_1C_1im][NTf_2]$, which is slightly higher than

their 1-alkyl-3-methylimidazolium analogues (4.2 *endo:exo*=4.2 in $[C_4C_1im][NTf_2]$). This observation suggests that the HBD ability of the cation does not satisfactorily to account for the selectivity. The possible reason is that the ILs such as $[C_4C_1C_1im][NTf_2]$ and $[C_4C_1py][NTf_2]$ have lower H-bonding ability but higher cohesive pressures and polarity, which is responsible for the higher *endo* selectivity.¹⁷⁰ H-bond-rich ILs have been synthesized for the Diels-Alder reaction of cyclopentadiene with diethyl maleate and it is found that such ILs are as active as metal catalysts but are significantly more active than the other ILs, indicating the role of H-bond in enhancing the reaction.¹⁷⁵

6.3 Acetalization reaction

Acetalization is often a multistep reaction when a carbonyl group is protected. The product acyclic acetals derived from secondary arylalcohols can be used in tandem with methyl acetals for the selective protection and deprotection of a carbonyl group in the presence of the other carbonyl-containing functionality.¹⁷⁶ However, the reaction is not thermodynamically favourable and reversible. Functional ILs with two acid sites as catalyst have been reported to effectively promote the reaction as shown in Scheme 2.¹⁷⁷



Scheme 2 Acetalization of secondary alcohols reaction.

The mechanism has been investigated by theoretical calculations.¹⁷⁸ It is shown that the N-H...O H-bond between an ion-pair and hemiacetal molecule stabilizes the pre-transition state (pre-TS). Fig. 17A shows the NBO donor-acceptor interactions (occupied n_O lone pair on hemiacetal OH oxygen with an unoccupied σ_{NH}^* antibonding NBO on protonated pyridine in O...HN alignment in the case). A large value of $E_{n \rightarrow \sigma^*}^{(2)}$ indicates energetically stabilization for the superposition of the occupied and unoccupied orbitals. The H-bond is also critical to stabilization of the TS (half-proton-transfer A...H...B) produced from proton transfer from pyridine to hemiacetal molecule. Three ILs exhibiting different activities observed in the experiment show different H-bonded donor-acceptor interactions.¹⁷⁸

It can be deduced from Fig. 17B that compared with other least-efficient ILs ($\Delta E_{nO} = 0.062$ a.u., $\Delta E_{n_{NH}^* \rightarrow n_{H}^*} = 0.321$ a.u., and $\Delta E_{nO} = 0.108$ a.u., $\Delta E_{n_{NH}^* \rightarrow n_{H}^*} = 0.333$ a.u.), the low perturbation of both O orbital ($\Delta E_{nO} = 0.060$ a.u.) and σ_{H}^* orbital ($\Delta E_{n_{H}^*} = 0.055$ a.u.) of the IL leads to the lowest energy gap (between the occupied and unoccupied NBOs) and the highest catalytic activity. In addition, from pre-TS to TS the changes in the occupancy of the transferred proton and antibonding orbital hanged from 0.492 to 0.503 e for the IL with the highest activity, while from 0.078 to 0.510 e and from 0.098 to 0.504 e for the other two ILs respectively. The results are in agreement with the calculated energy barriers from reactant to TS ($\Delta E_a = 6.7, 7.9$ and 25.1 kJ mol⁻¹).

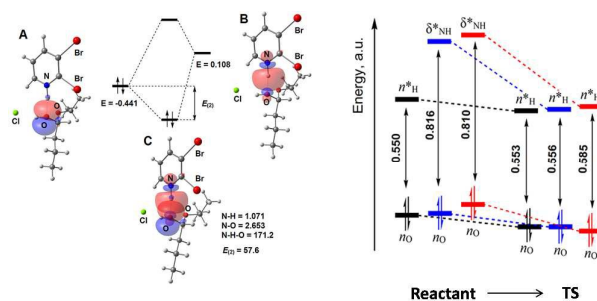
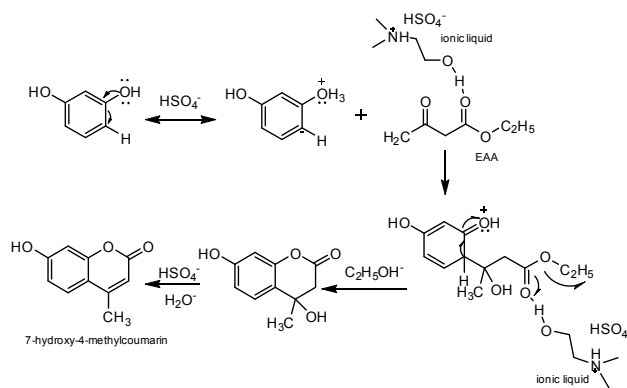


Fig. 17 NBO donor-acceptor energy diagram to stabilize the pre-TS and TS in the reaction between an ion-pair and a hemiacetal molecule. B Second-order stabilization energy $E_{n \rightarrow \sigma^*}^{(2)}$ (kcal/mol) and orbital energy E (atomic units). (Copyright 2015, American Chemical Society).¹⁷⁸

6.4 Other reactions enhanced by H-bonds

Knoevenagel reaction. The enhancement of the HBD ability of the cations and the hydrogen bond acceptor (HBA) ability of the anions can both lead to the increase in the catalytic activity of ILs. The cations form H-bond with aldehyde as electrophile to activate the C=O bond and the anions promote the active methylene compound to produce carboanion. Thus the ILs exhibit a dual function activation effect in the catalytic processes.¹⁷⁹

Pechmann reaction. A cholinium *N,N*-dimethylaminoethanol hydrosulfate ([N₁₁₂OH][HSO₄]) IL is found to be an efficient and reusable catalyst for the Pechmann condensation reaction under solvent-free conditions.¹⁸⁰ The UV-vis studies suggest that the increase of the acidity and the introduction of a hydroxyl group to the cation benefit the existence of the keto tautomer of ethyl acetoacetate, which then leads to the excellent performance of [N₁₁₂OH][HSO₄] in the mechanism proposed in Scheme 3.



Scheme 3 Proposed mechanism for Pechmann reaction catalyzed by [N₁₁₂OH][HSO₄] IL.¹⁸⁰

Nucleophilic substitution reaction. Nucleophilic substitution reactions of alcohols catalyzed by a zinc-based IL ([CHCl][ZnCl₂]) have been demonstrated to have the high conversion, high selectivity, easy separation procedure, good reusability and no use of excessive nucleophiles.¹⁸¹ This reaction is suggested to go through the carbocation mechanism detected by UV-vis

spectroscopy. This results implied that the hydroxyl group on the choline cation was the major inducement for the formation of special microstructures which could provide adequate stability for the carbocation in the reaction system and increase the reactivity and selectivity.

6.5 Dissolution of lignocellulosic biomass by H-bonding formation

Lignocellulosic biomass is the most abundantly available raw material on the earth,¹⁸² and is mainly composed of cellulose, hemicellulose and lignin. In 2002, Swatloski et al.⁴ reported that [C₄C₁im]Cl can effectively dissolve cellulose, which opened a new application of ILs. In recent years, a variety of ILs have been used to dissolve and pretreat lignocellulose¹⁸³, hemicellulose and lignin¹⁸⁴, even wheat, triticale, rice straw and wood.¹⁸⁵⁻¹⁸⁸ The natural form of cellulose is highly crystallized and embedded in a matrix of the polymers.²⁶ Overcoming this recalcitrance (i.e. the resistance of plant cell walls to deconstruction) is a limiting step for the utilization of lignocellulosic biomass.¹⁸⁹ The main recalcitrance for a crystalline cellulose microfibril is from three H-bonding interactions: intrachain O-H...O H-bonds along a single chain, interchain O-H...O H-bonds within a flat sheet, and intersheet C-H...O H-bonds between staggered glucan chains in two different sheets (Fig. 18).

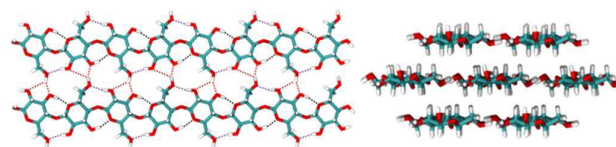


Fig. 18 The intrachain, interchain and intersheet H-bonds in cellulose.

From NMR and neutron scattering measurements, it was found that the solution of cellulose in ILs involves stoichiometric H-bonding interactions between hydroxyls of cellulose and anions^{190, 191}, which indicates that the molecular origin of the dissolution is the competition from H-bonds of cellulose and H-bonds between cellulose and ILs. Xu *et al.*¹⁹² speculated that ILs with anions having higher H-bond basicity and dipolarity possess the stronger ability of dissolution. The dissolution of polyols pentaerythritol (PET), a well-defined model compound of cellulose in ILs has been studied by IR spectroscopy^{193, 194}. It is shown that the dissolution is largely dependent on the ability of the anion to disrupt the H-bonding network of PET. However, the results of ¹³C NMR¹⁹⁵ implied that acidic protons on the imidazolium ring of the cations form C-H...O H-bond with linker oxygen of cellulose. This suggests that cations may play a role in the dissolution process. In order to dissect the role of H-bond in the dissolution of cellulose, MD simulations have been performed to reveal the mechanism. Liu *et al.*¹⁹⁶ found that interaction between the acetate anions ([OAc⁻]) and the hydroxyl group of the glucose three times stronger than that between water and hydroxyl group (Fig. 19A), actually indicating that the IL can disrupt the intrachain O-H...O H-bonds. In Fig. 19B, the distribution of torsion angles of glucose linkage (C₁-O₄-C₄-C₅, Ψ and C₅-C₁-O₄-C₄, Φ) in water and in IL was compared. It is clear that the majority of

the conformations falls in a broad basin centered around $(-80^\circ, -120^\circ)$ in water, which suggests that the water solvated polysaccharide chain has similar backbone conformations. However, the conformations in the IL are distributed in three distinct regions and the majority locates in a more confined region centered at $(-125^\circ, -125^\circ)$, which represents an extended polysaccharide structure.

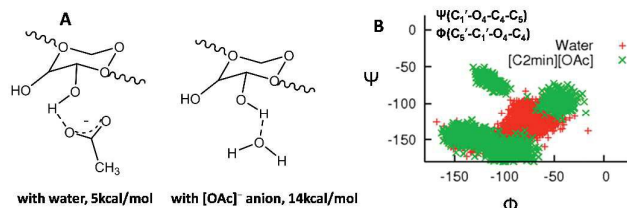


Fig. 19 A. the estimated H-bond strength in water and in [Emim][OAc]. B. the distribution of torsion angles of Φ - Ψ for the glucose linkage in polysaccharide chain (Copyright 2010, American Chemical Society).¹⁹⁶

MD simulation of a small cellulose bundle in $[C_4C_1im][OAc]$ IL suggests that the number of H-bonds gradually decreases at the surface layer of the bundle. This indicates that solvation leads to the breaking of interchain H-bonds at the surface.^{197, 198} Furthermore, Rabideau et al.^{199, 200} explored the transformation for small cellulose bundles in different ILs and proposed that anions

intensively bind to the hydroxyl groups of cellulose surface to form a negatively charged moiety, weakening the H-bonds between cellulose chains. Then due to the opposite charge attraction, cations can intercalate into the cellulose bunches to promote the separation of different cellulose chains as shown in Fig. 20A. In a recent study, Zhang et al.²⁰¹ carried out 500ns MD simulation of cellulose bunches in the $[C_2C_1im][OAc]$ IL and the complete cleavage of the chains was observed. After 350ns, the number of H-bonds of cellulose-cellulose and cellulose-ILs was no change, which indicates that the old intracellulose H-bonding network is replaced by the cellulose-IL H-bonds. However, the larger scale simulation for a cellulose microfibril revealed that the intersheet C-H...O H-bonds are the more robust and stronger component than other H-bonds. The number of intersheet H-bonds is a clear descriptor to distinguish the two allomorphs.²⁰² These results highlight the dominant role of the often-overlooked intersheet interactions giving rise to biomass recalcitrance. Fig. 20B shows the energy-minimized reaction path for the peeling off the corner glucan chains. Potential of mean force (PMF) for the peeling off a glucan chain from cellulose microfibril in $[C_4C_1im]Cl$ solvent shows clearly distinct from the PMF in water. The free energy reduction is 2.0kcal/mol for the peeling off per glucose residue, which explains the reason why the cellulose can be dissolved in IL but not in water.²⁰³

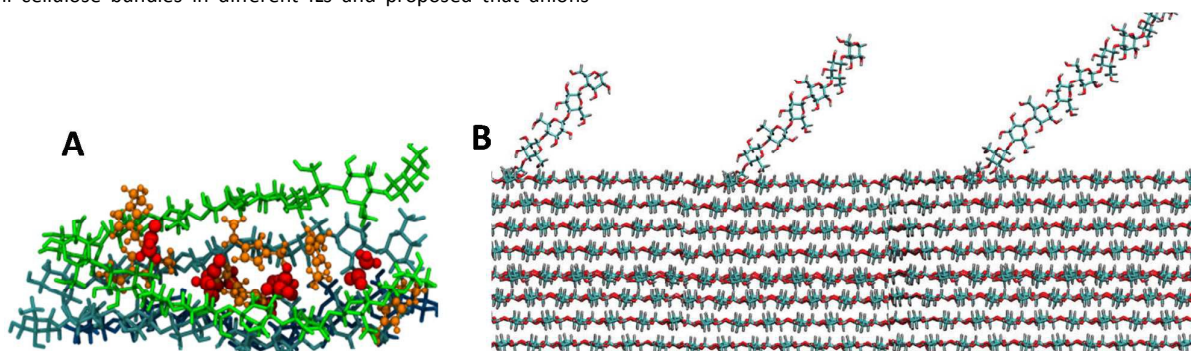
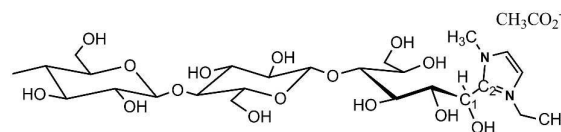


Fig. 20 MD simulation of cellulose deconstruction. A. Snapshot of a cellulose bunch with 7 chains in $[C_2C_1im][OAc]$ IL and cations and anions lead to the cleavage of the chains by H-bonds. B. Snapshots of the energy-minimized reaction path for peeling off the corner glucan chains from a cellulose microfibril with 36 glucan chains (Copyright 2011, American Chemical Society).²⁰³

During the dissolution of cellulose in ILs, the opening ring reaction should be taken into account. The cation is suggested to play an role in the reaction instead of forming direct strong H-bonds with cellulose.²⁰⁴ C-isotopic labeling and fluorescence labeling experiments have verified the hypothesis that a covalent bonding is formed between the C^2 carbon of imidazolium cation and the end of cellulose, as shown in Scheme 4.²⁰⁵ Zhang et al.²⁰⁶ found that the ring opening happened in $[C_2C_1im][OAc]$ may be due to the attack of HOAc on cellobiose and the subsequent formation of an intermediate. Then, nucleophilic attack by carbene on the C atom of the intermediate ring leads to the formation of covalent bond and opening of the ring.



Scheme 4 Proposed structure for a covalent binding of [Emim][OAc] to celloglucomer.

7. Summaries

In this article, we reviewed the H-bonds in ILs. From the above discussion, it is clear that the H-bond is never not essential for structures, properties and applications of ILs. The model of H-bond between cation and anion can be expressed as $(+)X^{\delta+}-H\cdots Y^{\delta-}(-)$, which leads to some uniquenesses in geometric, energetic and

electronic aspects compared with the conventional H-bond. The H-bonds in the imidazolium-based ILs show bifurcated and chelated geometric structures and the interaction energy is increased remarkably. From the AIM, MO and NBO analyses, it is found that the values of ρ_{BCP} and $\nabla^2\rho_{\text{BCP}}$ are well established parameters for characterization of H-bonds. FMO analysis shows that the HOMO and LUMO for the ion-pair are very similar to the isolated ion orbitals, however the deeper HOMOs exhibit σ symmetry, indicating strong interaction between a formal empty $\text{C}^2\text{-H } \sigma^*$ -bond orbital and the filled pAO of Cl^- anion. The delocalization energy $E_{n \rightarrow \sigma^*}^{(2)}$ measures the donor-acceptor capability and exhibits the same trend with strengths of H-bonds. Imidazolium salt ion-pairs with $[\text{BF}_4]^-$ and $[\text{PF}_6]^-$ anions have low $E_{n \rightarrow \sigma^*}^{(2)}$ values of 50-60 kJ/mol and show the weak H-bonds, while those with Cl^- and $[\text{NO}_3]^-$ anions have higher $E_{n \rightarrow \sigma^*}^{(2)}$ values of 110-180 kJ/mol and show the stronger H-bonds. The PILs have highest $E_{n \rightarrow \sigma^*}^{(2)}$ values of 250-320 kJ/mol and indicate the strongest H-bonding interaction. The uniqueness of H-bonds may stem from the cooperation with strong electrostatic force, dispersion and π interactions to balance the different interactions in varied environment. In crystal and liquid states, H-bonding network induces structural directionality and is responsible for ion stacking, aggregates and assembly in neat ILs and IL solutions, and so that ILs cannot be regarded as homogeneous solvents.

For the non-imidazolium-based ILs, the α -hydrogen is acidic and participates to form the weak H-bond with anion. However, for the PILs, the proton transfer between cation and anion leads to the stronger H-bonds and the formation of H-bonding network.

Experimentally, the low frequency spectroscopy provides the measurement for the H-bonds in ILs. By varying anions and cations, it is shown that the increasing interaction strength results in frequency shifts to higher wavenumbers due to the increase of force constant, indicating stronger interaction between the ion species. Also it is confirmed that H-bond contributes to local and directional nature of the interaction, and significantly influences the properties of ILs. H-bonding interactions lead to the decrease of melting points and viscosities, and then the fluidization of the ILs. The enthalpy of vaporization also correlates with the H-bond, stronger H-bond leads to the decrease of enthalpy of vaporization. H-bond plays important roles in enhancing reactions when ILs are used as catalyst and solvent. In CO_2 absorption, the anion-cation H-bonds influence to reduce energy barrier and lead to the easier reaction between CO_2 and the $-\text{NH}_2$ group. In the conversion, the H-bond between the epoxide ring and HBD makes a positive contribution on the activity of ILs to accelerate the ring opening of epoxide. H-bond also plays an important role in stabilizing TS, for example in acetalization reaction H-bond is critical to stabilize the TS for proton transfer from pyridine to hemiacetal molecule. In Diels-Alder reaction, the H-bond not only influences the reaction equilibrium but also increases *endo/exo* selectivity, and it has been found that strong H-bond increases the *endo* selectivity. In the mentioned Knoevenagel, Pechmann and nucleophilic substitution

reactions, the dual function of H-bond and the enhancement in the HBD ability of the cations and HBA ability of the anions results in the increase in the catalytic activity of the ILs.

An important utility of ILs is their application in the pre-treatment of lignocellulosic biomass, especially cellulose. Mechanism investigation suggests that the effect of H-bond is essential to the dissolution of cellulose. The formation of H-bonds between cellulose-IL deconstructs the intrachain, interchain and intersheet H-bonding network of cellulose. Although the H-bonds of anion-hydroxyl are main reason for the dissolution, the cation can form weak H-bond with the ether oxygen in cellulose, and the synergistic effect of cation and anion has been accepted extensively.

Acknowledgements

We thank the Projects supported by International S&T Cooperation Program of China (2014DFA61670) and National Natural Science Foundation of China (91534116).

References:

1. S. Zhang, J. Sun, X. Zhang, J. Xin, Q. Miao and J. Wang, *Chem. Soc. Rev.*, 2014, **43**, 7838-7869.
2. J. P. Hallett and T. Welton, *Chem. Rev.*, 2011, **111**, 3508-3576.
3. T. Le, V. C. Epa, F. R. Burden and D. A. Winkler, *Chem. Rev.*, 2012, **112**, 2889-2919.
4. R. P. Swatloski, S. K. Spear, J. D. Holbrey and R. D. Rogers, *J. Am. Chem. Soc.*, 2002, **124**, 4974-4975.
5. R. D. Rogers, *Nature*, 2007, **447**, 917-918.
6. E. F. Borra, O. Seddiki, R. Angel, D. Eisenstein, P. Hickson, K. R. Seddon and S. P. Worden, *Nature*, 2007, **447**, 979-981.
7. B. A. Rosen, A. Salehi-Khojin, M. R. Thorson, W. Zhu, D. T. Whipple, P. J. A. Kenis and R. I. Masel, *Science*, 2011, **334**, 643-644.
8. P. Bonhôte, A. P. Dias, N. Papageorgiou, K. Kalyanasundaram and M. Grätzel, *Inorg. Chem.*, 1996, **35**, 1168-1178.
9. J. S. Wilkes and M. J. Zaworotko, *J. Chem. Soc., Chem. Commun.*, 1992, 965-967.
10. C. Wang, X. Luo, H. Luo, D.-e. Jiang, H. Li and S. Dai, *Angew. Chem. Int. Ed.*, 2011, **50**, 4918-4922.
11. B. E. Gurkan, J. C. d. I. Fuente, E. M. Mindrup, L. E. Ficke, Brett F. Goodrich, E. A. Price, W. F. Schneider and J. F. Brennecke, *J. Am. Chem. Soc.*, 2010, **132**, 2116-2117.
12. X. Huang, C. J. Margulis, Y. Li and B. J. Berne, *J. Am. Chem. Soc.*, 2005, **127**, 17842-17851.
13. S. Zhang, Y. Chen, R. X.-F. Ren, Y. Zhang, J. Zhang and X. Zhang, *J. Chem. Eng. Data*, 2005, **50**, 230-233.
14. X. Han and D. W. Armstrong, *Acc. Chem. Res.*, 2007, **40**, 1079-1086.
15. Y. Qin, X. Lu, N. Sun and R. D. Rogers, *Green Chem.*, 2010, **12**, 968-971.
16. S. S. Y. Tan, D. R. MacFarlane, J. Upfal, L. A. Edye, W. O. S. Doherty, A. F. Patti, J. M. Pringle and J. L. Scott., *Green Chem.*, 2009, **11**, 339-345.

17. M. V. Fedorov and A. A. Kornyshev, *Chem. Rev.*, 2014, **114**, 2978-3036.
18. P. Hapiot and C. Lagrost, *Chem. Rev.*, 2008, **108**, 2238-2264.
19. K. Kirchner, T. Kirchner, V. Ivaništševa and M. V. Fedorova, *Electrochimica Acta*, 2013, **110**, 762-771.
20. V. Borgel, E. Markevich, D. Aurbach, G. Semrau and M. Schmidt, *J. Power Sources*, 2009, **189**, 331-336.
21. J. Xiang, F. Wu, R. Chen, L. Li and H. Yu, *J. Power Sources*, 2013, **233**, 115-120.
22. S. Li, J. L. Bañuelos, P. Zhang, G. Feng, S. Dai, G. Rotherc and P. T. Cummingsa, *Soft Matter*, 2014, **10**, 9193-9200.
23. M. Armand, F. Endres, D. R. MacFarlane, H. Ohno and B. Scrosati, *Nature Mater.*, 2009, **8**, 621-629.
24. J. L. Bideau, L. Viaub and A. Vioux, *Chem. Soc. Rev.*, 2011, **40**, 907-925.
25. A. Pinkert, K. N. Marsh, S. Pang and M. P. Staiger, *Chem. Rev.*, 2009, **109**, 6712-6728.
26. H. Wang, G. Gurau and R. D. Rogers, *Chem. Soc. Rev.*, 2012, **41**, 1519-1537.
27. K. Dong, G. Zhou, X. Liu, X. Yao and S. Zhang, *J. Phys. Chem. C*, 2009, **113**, 10013-10020.
28. S. Chen, K. Kobayashi, R. Kitaura, Y. Miyata and H. Shinohara, *ACS Nano*, 2011, **5**, 4902-4908.
29. S. Chen, G. Wu, M. Sha and S. Huang, *J. Am. Chem. Soc.*, 2007, **129**, 2416-2417.
30. T. Fukushima, A. Kosaka, Y. Ishimura, T. Yamamoto, T. Takigawa, N. Ishii and T. Aida, *Science*, 2003, **300**, 2072-2074.
31. R. D. Rogers and K. R. Seddon, *Science*, 2003, **302**, 792-793.
32. S. Zahn, F. Uhlig, J. Thar, C. Spickermann and B. Kirchner, *Angew. Chem. Int. Ed.*, 2008, **47**, 3639-3641.
33. K. Dong, Y. Song, X. Liu, W. Cheng, X. Yao and S. Zhang, *J. Phys. Chem. B*, 2012, **116**, 1007-1017.
34. P. B. Hitchcock, K. R. Seddon and T. Welton, *J. Chem. Soc. Dalton Trans.*, 1993, 2639-2643.
35. R. W. Berg, M. Deetlefs, K. R. Seddon, I. Shim and J. M. Thompson, *J. Phys. Chem. B*, 2005, **109**, 19018-19025.
36. S. A. Katsyuba, M. V. Vener, E. E. Zvereva, Z. Fei, R. Scopelliti, G. Laurency, N. Yan, E. Paunescu and P. J. Dyson, *J. Phys. Chem. B*, 2013, **117**, 9094-9105.
37. A. Yokozeki, D. J. Kasprzak and M. B. Shiflett, *Phys. Chem. Chem. Phys.*, 2007, **9**, 5018-5026.
38. K. Dong, S. Zhang, D. Wang and X. Yao, *J. Phys. Chem. A*, 2006, **110**, 9775-9782.
39. K. Dong and S. Zhang, *Chem. Eur. J.*, 2012, **18**, 2748-2761.
40. W. M. Reichert, J. D. Holbrey, R. P. Swatloski, K. E. Gutowski, A. E. Visser, M. Nieuwenhuyzen, K. R. Seddon and R. D. Rogers, *Crystal Growth & Design* 2007, **7**, 1106-1114.
41. K. Fumino, A. Wulf and R. Ludwig, *Angew. Chem. Int. Ed.*, 2008, **47**, 8731-8734.
42. K. Fumino, A. Wulf and R. Ludwig, *Angew. Chem. Int. Ed.*, 2008, **47**, 3830-3834.
43. K. Fumino, T. Peppel, M. Geppert-Rybczyńska, D. H. Zaitsau, J. K. Lehmann, S. P. Verevkin, M. Köckerling and R. Ludwig, *Phys. Chem. Chem. Phys.*, 2011, **13**, 14064-14075.
44. K. Fumino, S. Reimanna and R. Ludwig, *Phys. Chem. Chem. Phys.*, 2014, **16**, 21903-21929.
45. L. Crowhurst, P. R. Mawdsley, J. M. Perez-Arlandis, P. A. Saler and T. Welton, *Phys. Chem. Chem. Phys.*, 2003, **5**, 2790-2794.
46. C. Roth, S. Chatzipapadopoulos, D. Kerlé, F. Friedriszik, M. Lütgens, S. Lochbrunner, O. Kühn and R. Ludwig, *New J. Physics*, 2012, **14**, 105026.
47. S. Gründemann, A. Kovacevic, M. Albrecht, J. W. F. Robert and H. Crabtree, *Chem. Commun.*, 2001, 2274-2275.
48. K. S. Han, S. Li, E. W. Hagaman, G. A. Baker, P. Cummings and S. Dai, *J. Phys. Chem. C*, 2012, **116**, 20779-20786.
49. X. Song, H. Hamano, B. Minofar, R. Kanzaki, K. Fujii, Y. Kameda, S. Kohara, M. Watanabe, S.-i. Ishiguro and Y. Umebayashi, *J. Phys. Chem. B*, 2012, **116**, 2801-2813.
50. K. Fumino, V. Fossog, K. Wittler, R. Hempelmann and R. Ludwig, *Angew. Chem. Int. Ed.*, 2013, **52**, 2368-2372.
51. T. L. Greaves and C. J. Drummond, *Chem. Rev.*, 2008, **108**, 206-237.
52. J. Hunger, T. Sonnleitner, L. Liu, R. Buchner, M. Bonn and H. J. Bakker, *J. Phys. Chem. Lett.*, 2012, **3**, 3034-3038.
53. K. Fumino, A. Wulf and R. Ludwig, *Angew. Chem. Int. Ed.*, 2009, **48**, 3184-3186.
54. E. Bodo, S. Mangialardo, F. Ramondo, F. Ceccacci and P. Postorino, *J. Phys. Chem. B*, 2012, **116**, 13878-13888.
55. R. Hayes, S. Imberti, G. G. Warr and R. Atkin, *Angew. Chem. Int. Ed.*, 2012, **51**, 7468-7471.
56. H. Rodríguez and J. F. Brennecke, *J. Chem. Eng. Data*, 2006, **51**, 2145-2155.
57. L. Cammarata, S. G. Kazarian, P. A. Salter, T. Welton and A. K. Soper, *Phys. Chem. Chem. Phys.*, 2001, **3**, 5192-5200.
58. P. Stange, K. Fumino and R. Ludwig, *Angew. Chem. Int. Ed.*, 2013, **52**, 2990-2994.
59. W. Beichel, N. Trapp, C. Hauf, O. Köhler, G. Eickerling, W. Scherer and I. Krossing, *Angew. Chem. Int. Ed.*, 2014, **53**, 3143-3146.
60. R. P. Matthews, T. Welton and P. A. Hunt, *Phys. Chem. Chem. Phys.*, 2014, **16**, 3238-3253.
61. J. Dupont, *Acc. Chem. Res.*, 2011, **44**, 1223-1231.
62. P. Judeinstein, C. Iojoiu, J.-Y. Sanchez and B. Ancian, *J. Phys. Chem. B*, 2008, **112**, 3680-3683.
63. H. S. Kim, S. H. Ha, L. Sethaphong, Y.-M. Koo and Y. G. Yingling, *Phys. Chem. Chem. Phys.*, 2014, **16**, 2944-2953.
64. D. Lousa, A. M. Baptista and C. M. Soares, *Phys. Chem. Chem. Phys.*, 2013, **15**, 13723-13736.
65. K. Fumino, V. Fossog, P. Stange, D. Paschek, R. Hempelmann and R. Ludwig, *Angew. Chem. Int. Ed.*, 2015, **54**, 2792-2795.
66. K. Fumino and R. Ludwig, *J. Mol. Liq.*, 2014, **192**, 94-102.
67. A. J. Arduengo, H. V. R. Dias, D. A. Dixon, R. L. Harlow, W. T. Klooster and T. F. Koetzle, *J. Am. Chem. Soc.*, 1994, **116**, 6812-6822.
68. C. Boehme and G. Frenking, *J. Am. Chem. Soc.*, 1996, **118**, 2039-2046.
69. P. A. Hunt, B. Kirchner and T. Welton, *Chem. Eur. J.*, 2006, **12**, 6762-6775.
70. L. Crowhurst, P. R. Mawdsley, J. M. Perez-Arlandis, P. A. Salter and T. Welton, *Phys. Chem. Chem. Phys.*, 2003, **5**, 2790-2794.
71. S. Hayashi, R. Ozawa and H. Hamagushi, *Chem. Lett.*, 2003, **32**, 498-499.
72. M. Buhl, A. Chaumont, R. Schurhammer and G. Wipff, *J. Phys. Chem. B*, 2005, **109**, 18591-18599.

73. A. M. Magill and B. F. Yates, *Aust. J. Chem.*, 2004, **57**, 1205-1210.
74. W. Zhao, F. d. Leroy, B. Heggen, S. Zahn, B. Kirchner, S. Balasubramanian and F. Müller-Plathe, *J. Am. Chem. Soc.*, 2009, **131**, 15825-15833.
75. H. A. Every, A. G. Bishop, D. MacFarlane, G. Orädd and M. Forsyth, *Phys. Chem. Chem. Phys.*, 2004, **6**, 1758-1765.
76. K. Ueno, H. Tokuda and M. Watanabe, *Phys. Chem. Chem. Phys.*, 2010, **12**, 1649-1658.
77. L. Pauling, *The Nature of the Chemical bond*, NY: Cornell University Press Ithaca, 3rd edn., 1960.
78. E. Arunan, G. R. Desiraju, R. A. Klein, J. Sadlej, S. Scheiner, I. Alkorta, D. C. Clary, R. H. Crabtree, J. J. Dannenberg, P. Hobza, H. G. Kjaergaard, A. C. Legon, Benedetta Mennucci and D. J. Nesbitt, *Pure Appl. Chem.*, 2011, **83**, 1637-1641.
79. T. Steiner, *Angew. Chem. Int. Ed.*, 2002, **41**, 48-76.
80. G. Gilli and P. Gilli, *J. Mol. Struct.*, 2010, **972**, 2-10.
81. M. Mautner, *Chem. Rev.*, 2011, **112**, pr22-pr103.
82. P. A. Hunt, C. R. Ashworth and R. P. Matthews, *Chem. Soc. Rev.*, 2015, **44**, 1257-1288.
83. P. A. Hunt and I. R. Gould, *J. Phys. Chem. A*, 2006, **110**, 2269-2282.
84. S. Tsuzuki, H. Tokuda, K. Hayamizu and M. Watanabe, *J. Phys. Chem. B*, 2005, **109**, 16474-16481.
85. D. T. Bowron, C. D'Agostino, L. F. Gladden, C. Hardacre, J. D. Holbrey, M. C. Lagunas, J. McGregor, M. D. Mantle, C. L. Mullan and T. G. A. Youngs, *J. Phys. Chem. B*, 2010, **114**, 7760-7768.
86. M. Deetlefs, C. Hardacre, M. Nieuwenhuyzen, A. A. H. Padua, O. Sheppard and A. K. Soper, *J. Phys. Chem. B*, 2006, **110**, 12055-12061.
87. C. Hardacre, J. D. Holbrey, S. E. J. McMath, D. T. Bowron and A. K. Soper, *J. Chem. Phys.*, 2003, **118**, 273-279.
88. Z. P. Liu, S. P. Huang and W. C. Wang, *J. Phys. Chem. B*, 2004, **108**, 12978-12989.
89. B. Jeziorski, R. Moszynski and K. Szalewicz, *Chem. Rev.*, 1994, **94**, 1887-1930.
90. J. Schmidt, C. Krekeler, F. Dommert, Y. Zhao, R. Berger, L. D. Site and C. Holm, *J. Phys. Chem. B*, 2010, **114**, 6150-6155.
91. K. Wendler, F. Dommert, Y. Y. Zhao, R. Berger, C. Holmb and L. D. Site, *Faraday Discuss.*, 2012, **154**, 111-132.
92. K. Wendler, S. Zahn, F. Dommert, R. Berger, C. Holm, B. Kirchner and L. D. Site, *J. Chem. Theory Comput.*, 2011, **7**, 3040-3044.
93. P. Hobza and Z. Havlas, *Chem. Rev.*, 2000, **100**, 4253-4264.
94. N. R. Dhumal, H. J. Kim and J. Kiefer, *J. Phys. Chem. A*, 2009, **113**, 10397-10404.
95. N. R. Dhumal, K. Noack, J. Kiefer and H. J. Kim, *J. Phys. Chem. A*, 2014, **118**, 2547-2557.
96. B. L. Bhargava and S. Balasubramanian, *J. Chem. Phys.*, 2007, **127**, 114510.
97. F. Dommert, K. Wendler, R. Berger, L. D. Site and C. Holm, *ChemPhysChem*, 2012, **13**, 1625-1637.
98. T. Cremer, C. Kolbeck, K. R. J. Lovelock, N. Paape, R. Wölfel, P. S. Schulz, P. Wasserscheid, H. Weber, J. Thar, B. Kirchner, F. Maier and H.-P. Steinrück, *Chem. Eur. J.*, 2010, **16**, 9018-9033.
99. Y. Zhang and E. J. Maginn, *J. Phys. Chem. B*, 2012, **116**, 10036-10048.
100. P. Popelier, *J. Phys. Chem. A*, 1998, **102**, 1873-1878.
- D. Xu, Q. Yang, B. Su, Z. Bao, Q. Ren and H. Xing, *J. Phys. Chem. B*, 2014, **118**, 1071-1079.
102. K. Fumino, A. Wulfa and R. Ludwig, *Phys. Chem. Chem. Phys.*, 2009, **11**, 8790-8794.
103. F. Weinhold and C. R. Landis, *Valency and Bonding A Natural Bond Orbital Donor-Acceptor Perspective*, Cambridge University Press, Cambridge, 2005.
104. W. Wu, Y. LU, Y. Liu, H. Li, C. Peng, H. Liu and W. Zhu, *J. Phys. Chem. A*, 2014, **118**, 2508-2518.
105. Y. Wang, H. Li and S. Han, *J. Chem. Phys.*, 2006, **124**, 044504.
106. R. Ludwig, *Phys. Chem. Chem. Phys.*, 2015, **17**, 13790-13793.
107. J. S. Wilkes and M. J. Zaworotko, *J. Chem. Soc., Chem. Commun.*, 1992, 965-967.
108. J. S. Wilkes and M. J. Zaworotko, *Supramol. Chem.*, 1993, **1**, 191-193.
109. M. Deetlefs, C. Hardacre, M. Nieuwenhuyzen, O. Sheppard and A. K. Soper, *J. Phys. Chem. B*, 2005, **109**, 1593-1598.
110. M. V. Fedorovz and R. M. Lynden-Bell, *Phys. Chem. Chem. Phys.*, 2012, **14**, 2552-2556.
111. E. I. Izgorodina and D. R. MacFarlane, *J. Phys. Chem. B*, 2011, **115**, 14659-14667.
112. K. Matsumoto, R. Hagiwara, Z. Mazej, P. Benkič and B. Žemva, *Solid State Sci.*, 2006 **8**, 1250-1257.
113. X.-W. Li, J. Zhang, B. Dong, L.-Q. Zheng and C.-H. Tung, *Colloids Surf. A*, 2009, **335**, 80-87.
114. M. Brüssel, M. Brehm, A. S. Pensado, F. Malberg, M. Ramzan, A. Stark and B. Kirchner, *Phys. Chem. Chem. Phys.*, 2014, **14**, 13204-13215.
115. K. Dong, Q. Wang and S. Zhang, *Sci. China Chem.*, 2015, **58**, 495-500.
116. J. Dupont, *J. Braz. Chem. Soc*, 2004, **15**, 341-350.
117. K. Mizuse, N. Mikami and A. Fujii, *Angew. Chem. Int. Ed.*, 2010, **49**, 10119-10122.
118. J. N. Canongia Lopes and A. A. H. Padua, *J. Phys. Chem. B*, 2006, **110**, 3330-3335.
119. A. Triolo, O. Russina, H.-J. Bleif and E. Di Cola, *J. Phys. Chem. B*, 2007, **111**, 4641-4644.
120. F. C. Gozzo, L. S. Santos, R. Augusti, C. S. Consorti, J. Dupont and M. N. Eberlin, *Chem. Eur. J.*, 2004, **10**, 6187-6193.
121. G. R. Gupta, G. R. Chaudhari, P. A. Tomar, Y. Gaikwad, A. Rameez, G. H. Pandya, G. P. Waghulade and K. J. Patil, *Asian J. Chem.*, 2013, **25**, 8261-8265.
122. C. S. Consorti, P. A. Z. Suarez, R. F. deSouza, R. A. Burrow, D. H. Farrar, A. J. Lough, W. Loh, L. H. M. da Silva and J. Dupont, *J. Phys. Chem. B*, 2005, **109**, 4341-4349.
123. P. M. Lalli, Y. E. Corilo, G. F. de Sa, D. R. J., V. de Souza, G. H. M. F. souza, I. Campuzano, G. Ebeling, J. Dupont and M. N. Eberlin, *ChemPhysChem*, 2011, **12**, 1444-1447.
124. E. Mamontov, G. A. Baker, H. Luo and S. Dai, *ChemPhysChem*, 2011, **12**, 944-950.
125. B. A. D. Neto, L. S. Santos, F. M. Nachtigall, M. N. Eberlin and J. Dupont, *Angew. Chem. Int. Ed.*, 2006, **45**, 7251-7254.
126. H. K. Stassen, R. Ludwig, A. Wulf and J. Dupont, *Chem. Eur. J.*, 2015, **21**, 8324-8335.
127. W. Shi, K. Damodaran, H. B. Nulwalae and D. R. Luebkea, *Phys. Chem. Chem. Phys.*, 2012, **14**, 15897-15908.

128. B. Aoun, A. Goldbach, M. González, S. Kohara, D. L. rice and M.-L. Saboungi, *J. Chem. Phys.*, 2011, **134**, 104509.
129. X. Liu, G. Zhou, H. He, J. Wang and S. Zhang, *Ind. Eng. Chem. Res.*, 2015, **54**, 1681–1688.
130. T. Ramnia, D. D. Ino and J. A. C. Clyburne, *Chem. Commun.*, 2005, 325–327.
131. S. Seo, M. A. DeSilva, H. Xia and J. F. Brennecke, *J. Phys. Chem. B*, 2015, **119**, 11807–11814.
132. M. Quiroz-Guzman, J. Daniel P. Fagnant, X.-Y. Chen, C. Shi, J. F. Brennecke, G. S. Goff and W. RundE, *RSC Adv.*, 2014, **4**, 14840–14846.
133. N.-N. Wang, Q.-G. Zhang, F.-G. Wu, Q.-Z. Li and Z.-W. Yu, *J. Phys. Chem. B*, 2010, **114**, 8689–8700.
134. H. He, H. Chen, Y. Zheng, S. Zhang and Z. Yu, *Chem. Eng. Sci.*, 2015, **121**, 169–179.
135. Y. Lauw, M. D. Horne, T. Rodopoulos, N. A. S. Webster, B. Minofar and A. Nelson, *Phys. Chem. Chem. Phys.*, 2009, **11**, 11507–11514.
136. R. Hayes, S. Imberti, G. G. Warr and R. Atkin, *Angew. Chem. Int. Ed.*, 2013, **52**, 4623–4627.
137. K. Fumino, P. Stange, V. Fossog, R. Hempelmann and R. Ludwig, *Angew. Chem. Int. Ed.*, 2013, **52**, 12439–12442.
138. K. Fumino, V. Fossog, P. Stange, K. Wittler, W. Polet, R. Hempelmann and R. Ludwig, *ChemPhysChem*, 2014, **15**, 2604–2609.
139. D. F. Evans, E. W. Kaler and W. J. Benton, *J. Phys. Chem.*, 1983, **87**, 533–535.
140. D. F. Evans, A. Yamauchi, G. J. Wei and V. A. Bloomfield, *J. Phys. Chem.*, 1983, **87**, 3537–3541.
141. M. Allen, D. F. Evans and R. Lumry, *J. Solution Chem.*, 1985, **14**, 549–560.
142. D. F. Kennedy and C. J. Drummond, *J. Phys. Chem. B Lett.*, 2009, **113**, 5690–5693.
143. K. Fumino, K. Wittler and R. Ludwig, *J. Phys. Chem. B*, 2012, **116**, 9507–9511.
144. A. Wulf, K. Fumino and R. Ludwig, *Angew. Chem. Int. Ed.*, 2010, **49**, 449–453.
145. C. Roth, T. Peppel, K. Fumino, M. Köckerling and R. Ludwig, *Angew. Chem. Int. Ed.*, 2010, **49**, 10221–10224.
146. K. Fumino, A. Wulf, S. P. Verevkin, A. Heintz and R. Ludwig, *ChemPhysChem*, 2010, **11**, 1623–1626.
147. P. A. Hunt, *J. Phys. Chem. B*, 2007, **111**, 4844–4853.
148. R. Ludwig and D. Paschek, *ChemPhysChem*, 2009, **10**, 516–519.
149. J. M. Slattery, C. Daguene, P. J. Dyson, T. J. Schubert and I. Krossing, *Angew. Chem. Int. Ed.*, 2007, **46**, 5384–5388.
150. E. I. Izgorodina, R. Maganti, V. Armel, P. M. Dean, J. M. Pringle, K. R. Seddon and D. R. MacFarlane, *J. Phys. Chem. B*, 2011, **115**, 14688–14697.
151. Y. Zhang and E. J. Maginn, *Phys. Chem. Chem. Phys.*, 2012, **14**, 12157–12164.
152. O. Borodin, *J. Phys. Chem. B* 2009, **113**, 12353–12357.
153. S. P. Verevkin, *Angew. Chem. Int. Ed.*, 2008, **47**, 5071–5074.
154. D. H. Zaitsau, G. J. Kabo, A. A. Strechan, Y. U. Paulechka, A. Tschersich, S. P. Verevkin and A. Heintz, *J. Phys. Chem. A*, 2006, **110**, 7303–7306.
155. M. A. A. Rocha and L. M. N. B. F. Santos, *Chem. Phys. Lett.*, 2013, **585**, 59–62.
156. W. Xu, E. I. Cooper and C. A. Angell, *J. Phys. Chem. B*, 2003, **107**, 6170–6178.
157. M. Yoshizawa, W. Xu and C. A. Angell, *J. Am. Chem. Soc.*, 2003, **125**, 15411–15419.
158. V. N. Emel'yanenko, G. Boeck, S. P. Verevkin and R. Ludwig, *Chem. Eur. J.*, 2014, **20**, 11640–11645.
159. J. Stoimenovski, E. I. Izgorodina and D. R. MacFarlane, *Phys. Chem. Chem. Phys.*, 2010, **12**, 10341.
160. J.-P. Belieres and C. A. Angell, *J. Phys. Chem. B*, 2007, **111**, 4926–4937.
161. A. Brandt, J. Gräsvik, J. P. Hallett and T. Welton, *Green Chem.*, 2013, **15**, 550–583.
162. T. L. Greaves and C. J. Drummond, *Chem. Soc. Rev.*, 2008, **37**, 1709–1726.
163. L. A. Blanchard, Z. Gu and J. F. Brennecke, *J. Phys. Chem. B*, 2001, **105**, 2437–2444.
164. E. D. Bates, R. D. Mayton, I. Ntai and J. James H. Davis, *J. Am. Chem. Soc.*, 2002, **124**, 926–927.
165. M. D. Soutullo, C. I. Odum, B. F. Wicker, C. N. Henderson, A. C. Stenson and J. H. Davis, *Chem. Mater.*, 2007, **19**, 3581–3583.
166. K. Fukumoto, M. Yoshizawa and H. Ohno, *J. Am. Chem. Soc.*, 2005, **127**, 2398–2399.
167. J. Q. Wang, J. Sun, W. G. Cheng, K. Dong, X. P. Zhang and S. J. Zhang, *Phys. Chem. Chem. Phys.*, 2012, **14**, 11021–11026.
168. J. Sun, J. Ren, S. Zhang and W. Cheng, *Tetrahedron Lett.*, 2009, **50**, 423–426.
169. T. Welton and P. Wasserscheid, *Ionic Liquids in Synthesis*, VCH-Wiley, Weinheim, 2007.
170. C. Chiappe, M. Malvaldi and C. S. Pomelli, *Green Chem.*, 2010, **12**, 1330.
171. A. P. Abbott, G. Capper, D. L. Davies, R. K. Rasheed and V. Tambyrajah, *Green Chem.*, 2002, **4**, 24–26.
172. C. Chiappe, M. Malvaldi and C. S. Pomelli, *J. Chem. Theory Comput.*, 2010, **6**, 179–183.
173. X. Zhua, J. Liub, Dongju Zhang and C. Liu, *Computational and Theoretical Chemistry*, 2012, **996**, 21–27.
174. A. Cerda-Monje, A. Aizman, R. A. Tapia, C. Chiapped and R. Contreras, *Phys. Chem. Chem. Phys.*, 2012, **14**, 10041–10049.
175. K. Erfurt, I. Wandzik, K. Walczak, K. Matuszek and A. Chrobok, *Green Chem.*, 2014, **16**, 3508–3514.
176. M. Kotke, Schreiner and P.R.Acid-Free, *Tetrahedron*, 2006, **62**, 434–439.
177. D. Li, F. Shi, J. Peng, S. Guo and Y. Deng, *J. Org. Chem.*, 2004, **69**, 3582–3585.
178. M. Romyantsev, N. S. Sitnikov and N. V. Somov, *J. Phys. Chem. A*, 2015, **119**, 4108–4117.
179. A. Zhu, R. Liu, L. Li, L. Li, L. Wang and J. Wang, *Catal. Today*, 2013, **200**, 17–23.
180. Y. Zhang, A. Zhu, Q. Li, L. Li, Y. Zhao and J. Wang, *RSC Adv.*, 2014, **4**, 22946–22950.
181. A. Zhu, L. Li, J. Wang and K. Zhuo, *Green Chem.*, 2011, **13**, 1244–1250.
182. H. Tadesse and R. Luque, *Energy Environ. Sci.*, 2011, **4**, 3913–3929.
183. K. C. Badgujar and B. M. Bhanage, *Bioresour Technol*, 2015, **178**, 2–18.
184. X. Hou, T. J. Smith, N. Li and M.-H. Zong, *Biotechnol Bioeng*, 2012, **109**, 2484–2493.
185. T. A. Nguyen, K. R. Kim, S. J. Han, H. Y. Cho, J. W. Kim, S. M. Park, J. C. Park and S. J. Sim, *Bioresour Technol*, 2010, **101**, 7432–7438.

Journal Name

ARTICLE

186. Q. Li, Y.-C. He, M. Xian, G. Jun, X. Xu, J.-M. Yang and L.-Z. Li, *Bioresour Technol*, 2009, **100**, 3570-3575.
187. D. Fu, G. Mazza and Y. Tamaki, *J. Agr. Food Chem.*, 2010, **58**, 2915-2922.
188. C. E. Wyman, B. E. Dale, R. T. Elander, M. Holtzapple, M. R. Ladisch, Y. Y. Lee, C. Mitchinson and J. N. Saddler, *Biotechnol. Progr.*, 2009, **25**, 333-339.
189. M. E. Himmel, S. Y. Ding, D. K. Johnson, W. S. Adney, M. R. Nimlos, J. W. Brady and T. D. Foust, *Science*, 2007, **315**, 804-807.
190. R. C. Remsing, R. P. Swatloski, R. D. Rogers and G. Moyna, *Chem. Commun.*, 2006, 1271-1273.
191. T. G. A. Youngs, J. D. Holbrey, C. L. Mullan, S. E. Norman, M. C. Lagunas, C. D'Agostino, M. D. Mantle, L. F. Gladden, D. T. Bowron and C. Hardacre, *Chem. Sci.*, 2011, **2**, 1594-1605.
192. A. Xu, J. Wang and H. Wang, *Green Chem.*, 2010, **12**, 268-275.
193. Z. Papanyan, C. Roth, K. Wittler, S. Reimann and R. Ludwig, *ChemPhysChem*, 2013, **14**, 3667-3671.
194. Z. Papanyan, C. Roth, D. Paschek and R. Ludwig, *ChemPhysChem*, 2011, **12**, 2400-2404.
195. B. Lu, A. Xu and J. Wang, *Green Chem.*, 2014, **16**, 1326-1335.
196. H. Liu, K. L. Sale, B. M. Holmes, B. A. Simmons and S. Singh, *J. Phys. Chem. B*, 2010, **114**, 4293-4301.
197. K. M. Gupta, Z. Hu and J. Jiang, *Polymer*, 2011, **52**, 5904-5911.
198. K. M. Gupta, Z. Hu and J. Jiang, *RSC Adv.*, 2013, **3**, 12794-12801.
199. B. D. Rabideau, A. Agarwal and A. E. Ismail, *J. Phys. Chem. B*, 2013, **117**, 3469-3479.
200. B. D. Rabideau, A. Agarwal and A. E. Ismail, *J. Phys. Chem. B*, 2014, **118**, 1621-1629.
201. Y. Li, X. Liu, S. Zhang, Y. Yao, X. Yao, J. Xu and X. Lu, *Phys. Chem. Chem. Phys.*, 2015, **17**, 17894-17905.
202. A. S. Gross and J.-W. Chu, *J. Phys. Chem. B*, 2010, **114**, 13333-13341.
203. H. M. Cho, A. S. Gross and J.-W. Chu, *J. Am. Chem. Soc.*, 2011, **133**, 14033-14041.
204. A. M. Fernandes, M. A. A. Rocha, M. G. Freire, I. M. Marrucho, J. A. P. Coutinho and L. M. N. B. F. Santos, *J. Phys. Chem. B*, 2011, **115**, 4033-4041.
205. G. Ebner, S. Schiehser, A. Potthast and T. Rosenau, *Tetrahedron Lett.*, 2008, **49**, 7322-7324.
206. Y. Yao, Y. Li, X. Liu, X. Zhang, J. Wang, X. Yao and S. Zhang, *Chin. J. Chem. Eng.*, , **Accepted**.